# METHODS OF GROWING CRYSTALS FROM AQUEOUS SOLUTION AND NUCLEAR MAGNETIC RESONANCE

By

FRANK HOLUJ

A Thesis
Submitted in Partial Fulfilment of
the Requirements for the Degree of
Master of Science
in the Department of Physics

McMaster University
May, 1956

## ACKNOWLEDGEMENTS

The author would like to express his sincerest thanks to Dr. H. E. Petch for his guidance and his constant interest at all stages of this research.

Mr. T. H. Bryden and Mr. W. McMicking of the Machine Shop executed the intricate crystal attachments.

This research was made possible by the assistantship from the Physics Department, by the "Cominco" fellowship from the Consolidated Mining and Smelting Company of Canada Limited, Trail, British Columbia and by the research grant to Dr. H. E. Petch from the Defence Research Board.

TABLE OF CONTENTS

SECTION I

SUBJECT — PAGE

SECTION II

## LIST OF ILLUSTRATIONS

## LIST OF TABLES

# ABSTRACT

Large single crystals, as nearly perfect as possible, are required for magnetic resonance studies of the solid state. A limited number of substances occur naturally in crystals of sufficient size or purity for this type of experiment. Most of the nuclear magnetic resonance work done to date on single crystals has been performed using naturally occurring crystals. Section I of this thesis describes methods used to grow suitable crystals artificially, thus extending the scope of the magnetic resonance experiments.

The orthorhombic sodium dihydrogen orthophosphate dihydrate has been produced in large single crystals which were used subsequently in the study of the nuclear magnetic resonance absorption spectrum of $Na^{23}$ in this crystal. The spectrum was observed as the crystal was rotated about the three crystallographic axes which are mutually perpendicular for the orthorhombic case. A maximum of twelve lines were observed when neither of the crystallographic axes were perpendicular to the external magnetic field. The number of lines was reduced to six when one of the axes was made perpendicular to the field, while only three lines were observed when two crystallographic axes were made perpendicular to the external magnetic field.

These observed numbers of lines were interpreted by assuming four $Na^{23}$ sites, possessing identical eigenvalues and differing only in their orientation. These four sites are related by three mutually perpendicular two-fold rotation axes, each of which must be parallel

to one of the three crystallographic axes. This interpretation is in complete accord with the space group P222 assigned to $NaH_2PO_4 2H_2O$ from morphological data. The complete set of properties of the quadrupole coupling tensor was determined at each of the $Na^{23}$ sites. The value of the quadrupole coupling constant $\frac{eQ\,\phi_{zz}}{h}$ where Q is the nuclear quadrupole moment and $\phi_{zz}$ is the largest principle value of the electric field gradient tensor is:

$$1179.0 \pm 0.5 \text{ kc/sec.}$$

The value of the asymmetry parameter $\eta$ defined as $\frac{\phi_{xx} - \phi_{yy}}{\phi_{zz}}$ is:

$$0.466 \pm 0.005$$

The table of the direction cosines of the principle axes of the electric field gradient tensor with respect to the crystallographic axes appear in Table VII.

# I. CRYSTAL GROWING METHODS

In recent years the production of large single crystals has become important not only for pure research experiments but also for industrial applications and as a result much work has been done on this problem. There are four fundamentally different methods for growing single crystals. These are:

1) Controlled cooling of the melt so that the material crystallizes into one crystal.
2) Controlled cooling of the vapour of an easily sublimable substance so that single crystals are deposited.
3) Some chemical reactions, when suitably controlled, can be made to yield crystals.
4) Controlled cooling of a solution also yields crystals in varying degrees of purity and size.

Of the methods quoted above, 3) and 4) are the simplest since they do not require complicated apparatus, but they do not always yield satisfactory results. Method 1) produces excellent crystals of large size and very high purity but is limited to materials which do not decompose at temperatures near their melting point. Method 2) is rarely used except in isolated cases when other methods fail to give satisfactory results.

We have used method 3) to produce crystalline calcium hydroxide. The reactants NaOH and $CaCl_2$ were permitted to diffuse into one another with the result that $Ca(OH)_2$ was generated at a very slow rate. Method 4) has also been tried in this case except that instead of cooling the saturated solution of $Ca(OH)_2$ it was warmed because $Ca(OH)_2$ has a negative temperature solubility gradient.

In the case of the primary alkali orthophosphates which we also tried to obtain in the form of large crystals, method 4) has been used exclusively, because all the salts belonging to this class are extremely soluble in water. This method of growing large crystals of these salts has proved to be satisfactory, especially in the case of sodium dihydrogen orthophosphate dihydrate.

# CHAPTER I

## THEORIES OF CRYSTAL GROWTH MECHANISMS

The mechanism of crystal growth has never been elucidated satisfactorily. This is not surprising because the crystal growth is a surface phenomenon and our knowledge of the processes occurring on surfaces is very limited. Pierre Curie (1) was the first to treat crystal growth thermodynamically. His theory is an extension of Gibb's general theory of capillary action. The free energy function of a crystal consists only of a term belonging to the surface free energy. Other terms vanish because a crystal is incompressible. Curie assigns different surface tension energies to different faces denoted by $A_1$, $A_2$. The system then behaves in such a way that the expression 1 is minimum:

$$A_1 \cdot S_1 + A_2 \cdot S_2 + \ldots\ldots = \text{minimum} \qquad \ldots\ldots 1$$

Si is the surface area in question. The expression 1 is known as Curie's Law. Curie's theory was re-examined by several workers. Among them More and Ritzel (2) originated an interesting theory based on different solubility pressures existing at different surfaces. Under certain circumstances their expression reduces to Curie's Law. In the light of the theory of More and Ritzel, the growing crystal faces are continually reshaped by dissolution - a fact that contradicts the experimental observation. Valelon (3), for example, kept a crystal in a just saturated solution for months without observing a change in the shape of the crystal. Another difficulty is encountered in this theory, namely, that it does not predict the effect of presence of other faces adjacent to the growing face.

Noyes and Whitney (4) applied the diffusion theory to crystal growth. In their original communication they worked out a detailed mechanism of dissolution phenomena as well as crystal growth. According to their theory the rate of dissolution is given by the expression:

$$\frac{dx}{dt} = KS\,(Co - C_2) \qquad \ldots\ldots\ 2$$

A similar expression holds for rate of growth. In 2, K is the rate constant which assumes different numerical values for dissolution and for growth. Co is the saturation concentration to which the surface S is exposed and $C_2$ is the bulk concentration. As can be seen from equation 2, the rate of dissolution (and growth) is controlled by diffusion. While equation 2 accounted well for the dissolution phenomena, it failed when applied to growth. Nerust (5) introduced explicitly the diffusion constants D and d into equation 2:

$$\frac{dx}{dt} = DS\,\frac{Co - C_2}{d} \qquad \ldots\ldots\ 3$$

where $\frac{Co - C_2}{d}$ is the concentration gradient, D the diffusion coefficient and S is the area of the surface in question. Though the expression 3 accounts for crystal growth in a qualitative way, it fails to account for the anisotropy of crystal growth. The latter can be introduced, assuming one of the following:

(a) the reaction at the surface is finite and not infinitely fast as assumed in 3,

(b) the $\frac{Co - C_2}{d}$ varies from face to face - an unsatisfactory assumption, devoid of experimental foundations,

(c) the saturation Co, varies from face to face.

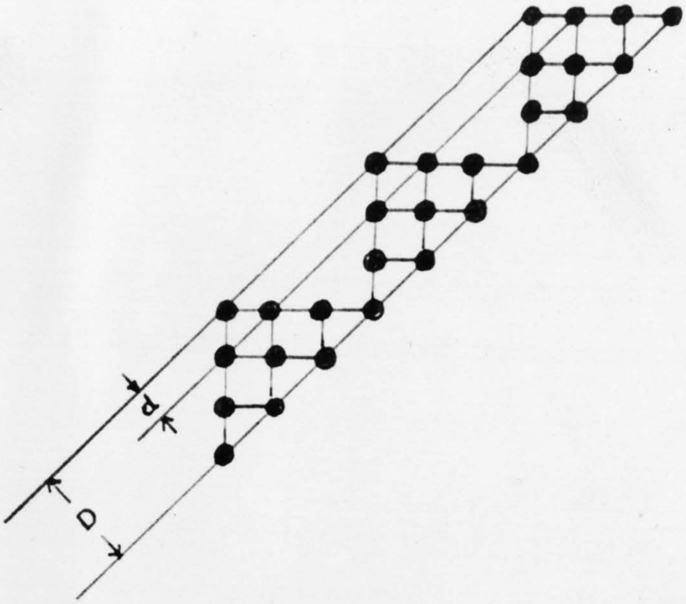

Fig. 1

Separation of planes on a growing crystal face.

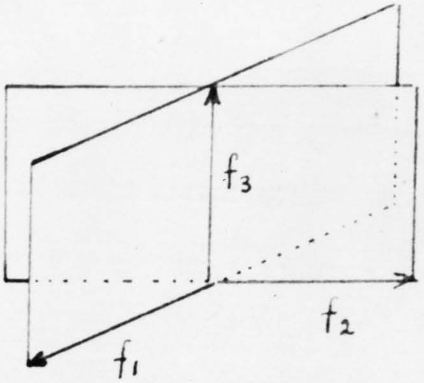

Fig. 2.

Direction of attractive forces on growing crystal face.

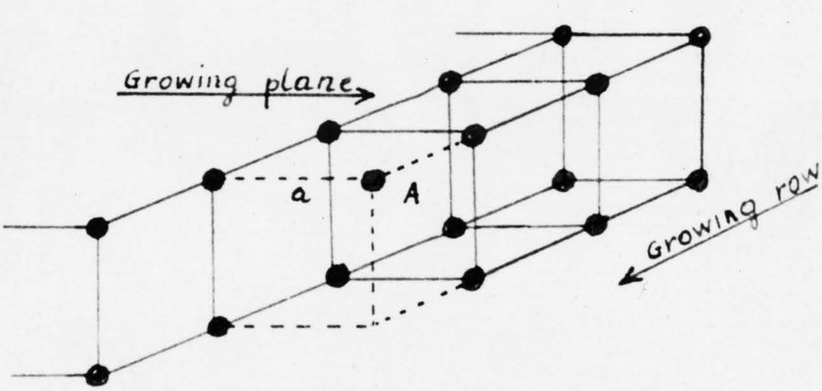

Fig. 3.

Growth of crystal planes by a successive addition of particles.

The possibility (c) was incorporated in an expression:

$$\frac{dx}{dt} = S \frac{k \frac{D}{S}}{k + \frac{D}{S}} (C_2 - Co) \qquad \text{.....} \; 4$$

due to Berthoud (6). Here k, the velocity of crystallization constant assumes different values for various faces and $s = d$. The expression 4 again proved unsatisfactory, for example, among other things, because the velocity of crystallization has been observed to be a polymolecular reaction and not, as 4 indicated, a unimolecular reaction. (See, for example, J. D. Jenkins, J. Am. Chem. Soc. 903, <u>47</u>, 1925).

The above theories were based on experimental evidences that totally ignored the fine structure of a crystal. The application of X-rays marked the beginning of a new subject, X-ray crystallography, which gives information useful for solving the microscopic structure of crystals. This knowledge gave birth to the three theories most favoured today. We must view them in a critical light and must not give them the mantle of infallibility, for crystal growth is essentially a surface phenomenon and our knowledge of fine structure of surfaces is greatly limited.

Bravais put forward in 1866 a theory which is surprisingly close to the modern view - that the velocity of growth is proportional to the reticular density of the ions or molecules on the surface in question. Niggli (7) elaborated the theory in the following way. Referring to Fig. 1, consider a growing surface (hkl) (Fig. 1), whose disturbed layer is $D_{hkl}$, $d_{hkl}$ is the separation of the planes on the surface (hkl). We see that the reticular density is proportional to $D_{hkl}$. Niggli gives a formula to be used in calculating $D_{hkl}$:

$$D_{hkl} = (h - 1)\ d_{hkl}\ h\ k\ l \qquad \ldots\ldots 5$$

It is possible to assign an order of importance of the face (hkl) during the process of growth, and the theory gives a reasonably good account of the crystal habit.

Kossel (8) assumed the crystal in equilibrium with solution. The potential energy of each particle is considered a simple function of its distance from the neighbouring particles. The potential energy is divided into 3 parts as shown in Fig. 2. As seen, the potential energy is given by:

$$f_0 = f_1 + f_2 + f_3$$

It is possible to work out an order of importance of the growing surfaces. Thus, for a simple cubic homopolar crystal consider a be the distance from the nearest neighbours, then $\sqrt{2}a$ and $\sqrt{3}a$ are the distances from other particles not in the immediate neighbourhood. Kossel neglects the presence of more distant particles.

The potential energy of a particle A at the growing row is:

$$\begin{aligned} f_1 &= /1/0/0/ \\ f_2 &= /1/2/0/ \\ f_3 &= /1/4/4/ \\ f_{OG} &= /3/6/4/ \end{aligned}$$

where the figures represent the number of neighbours at distances a, $\sqrt{2}a$, $\sqrt{3}a$ respectively. For a row to start we have:

$$f_{OR} = f_2 + f_3 = /2/6/4/$$

For a new plane to start the following holds:

$$f_{OD} = f_3 = /1/4/4/$$

We can visualize the process of growth as a rapid growth of rows. Since $f_{OG}$ $f_{OR}$ $f_{OP}$ the controlling factor in the rate of growth is determined by the ease with which a plane can be started. We see also that a likely spot where a plane is to start is midface > edge > corner. We can also deduce that (110) grows more rapidly than (100) since $f_{3_{(110)}} > f_{3_{(100)}}$

When considering a heteropolar crystal in the light of Kossels' theory, we have to take account of positive and negative ions. Basing our calculations along similar lines to those in the case of a heteropolar crystal we find:

$$f_{1_{(100)}} = 0.693$$
$$f_{2_{(100)}} = 0.1144$$
$$f_{3_{(100)}} = 0.0662$$

also $f_{0_{(100)}} > f_{0_{(100)}}$. We see that the starting point for a new plane during growth now becomes corner edge midface.

Stranski (9) has worked out a theory of the growth of a NaCl crystal assuming surface strains. The strains are probable since it is observed that the bond-lengths in the NaCl molecule in the vapour state is $2.3 \times 10^{-8}$ as compared to $2.8 \times 10^{-8}$ in the interior of the crystal. The growing surface is highly strained, the strains disappearing as the superimposed layers are added. Stranski assumes that the potential energy of the particles is made up (a) electrostatic and (b) repulsive potential energies. The latter term assumes the form given to it by Born (10). Stranski then sets out to calculate the energies of the 27 different positions on a growing (100) face of the cube.

Stranski and Kossel have outlined theories which are in many ways similar. Both lead to an important conclusion that the only possible faces in a NaCl crystal are (100), (010) etc. Other faces are made up of the striations of the elementary cubes. We have seen that the diffusion must and does play its part in the velocity with which the crystal grows. Where does it enter in Kossel's or Stranski's theories? We saw in Kossel's picture that the lime separating the deposition of a lone particle on a growing surface and a completion of a face are the determining factors in the velocity of growth. Thus, while one face enjoys a lull of activity, other surfaces may be arrested in their growth for a short while. Different concentrations at different surfaces are thus possible.

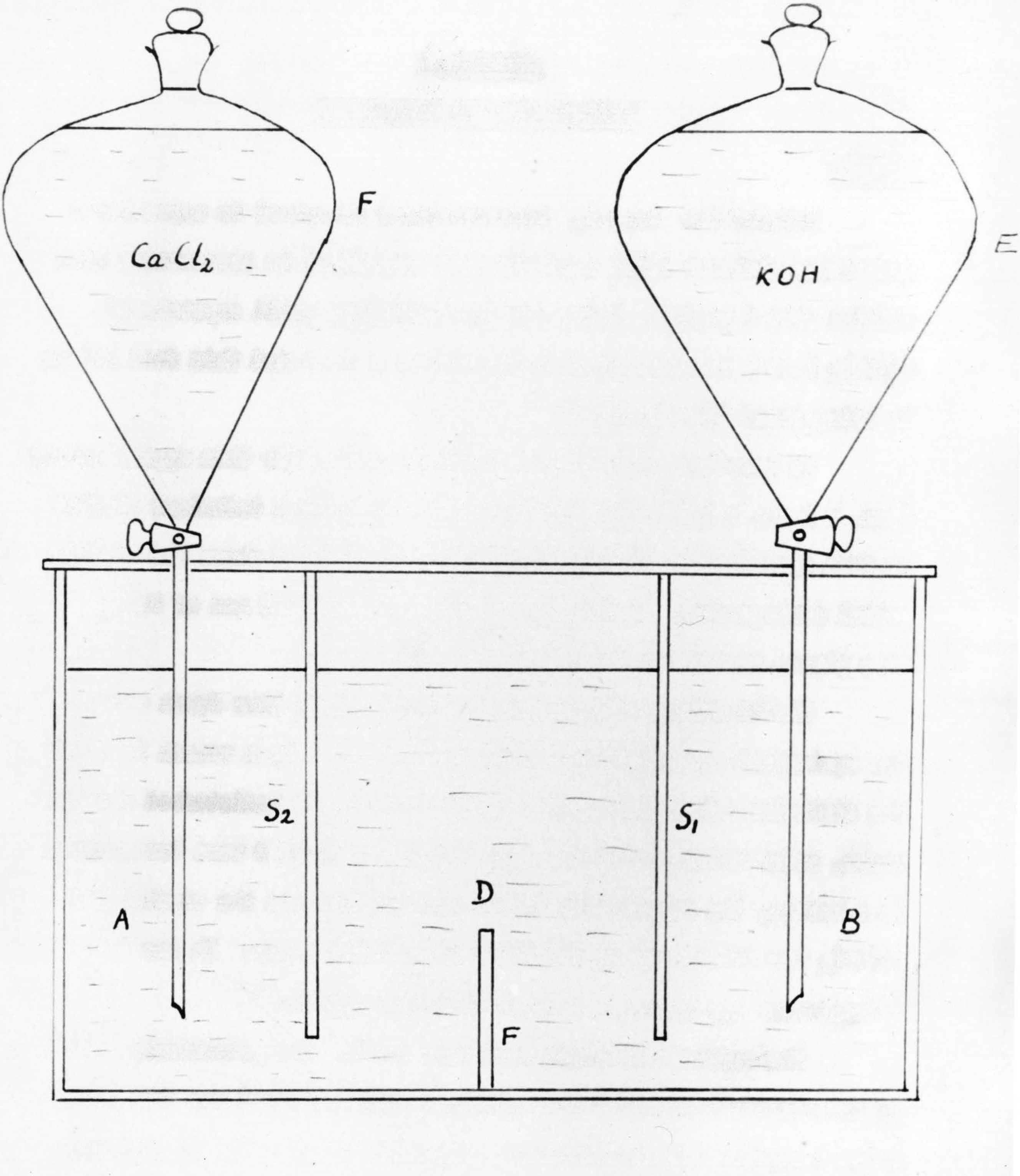

Fig 5.

Apparatus used to grow $Ca(OH)_2$ crystals by diffusion. method

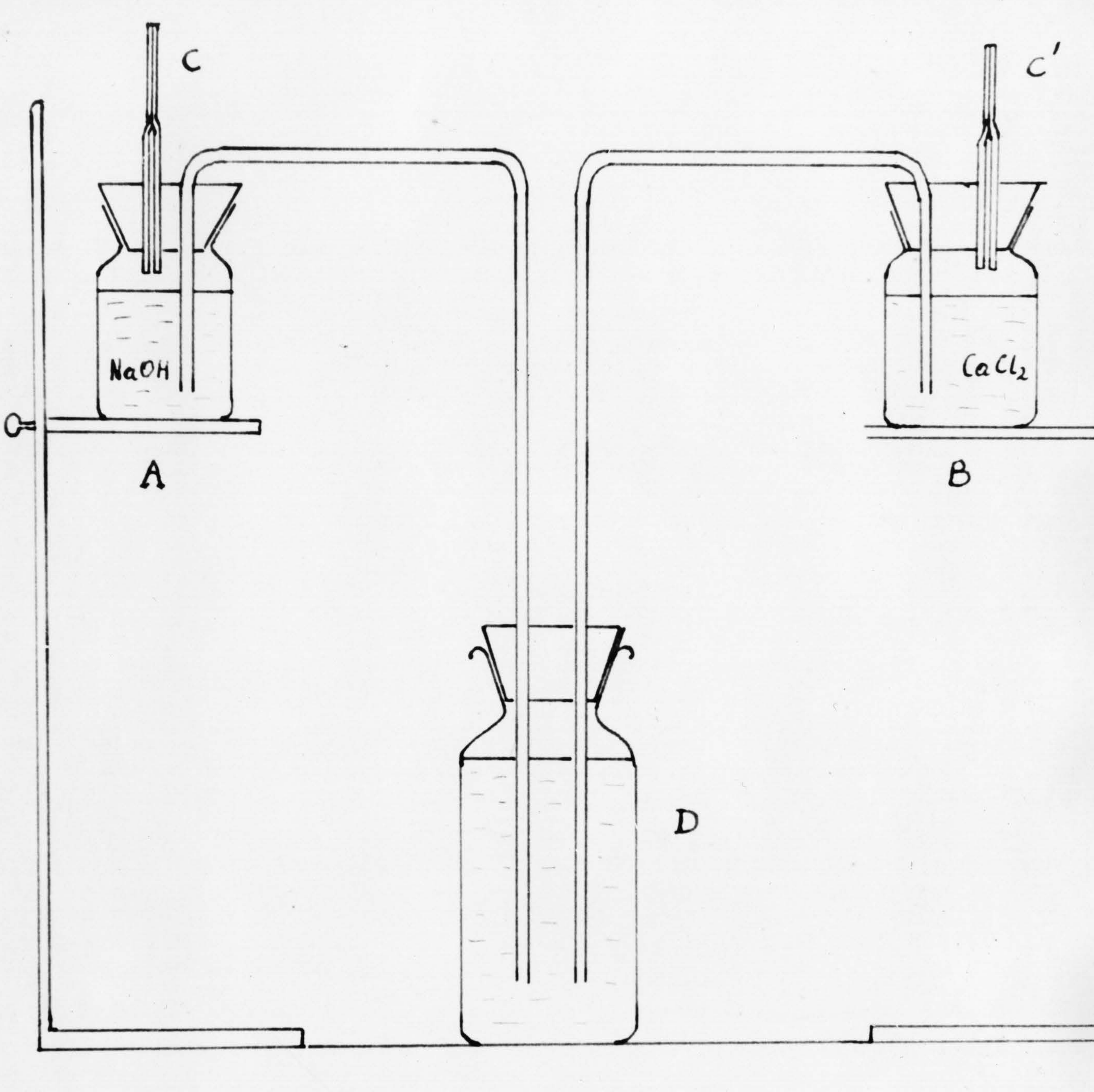

Fig. 4.

Apparatus used to grow $Ca(OH)_2$ crystals by diffusion method.

# CHAPTER II

## CRYSTAL GROWING TECHNIQUES

### $Ca(OH)_2$

Portlandite $Ca(OH)_2$ does not occur in nature in appreciable quantities although small crystals have been found in association with calcium salt deposits. Under certain conditions small crystals of $Ca(OH)_2$ have been found to form in portland cement and this fact led to it being named "portlandite".

We have been able to grow small (never bigger than approximately 3 mm. x 3 mm. x 1/2 mm.) crystals of $Ca(OH)_2$ using a technique similar to that described by Ashton and Wilson (11). Fig. 5 shows the experimental arrangement. Equally normal solutions of $NaOH$ and of $CaCl_2$ were placed in bottles A and B.

The capillary tubings C and C' were cut to have equal bore. The equivalent concentrations used were 7.01N. D is a vessel in which the diffusion takes place. The apparatus was left undisturbed for two weeks, after which period the contents of the flask D were transferred to a beaker, the supernatant liquid was decanted and the crystalline $Ca(OH)_2$ was dried between the folds of a filter paper. It was left in a dessicator containing a carbon dioxide absorbent.

The crystals obtained were very small. The preliminary mixing of the reactants caused a precipitation that destroyed the chances of a small crystal seed to grow to a bigger size. The rate of syphoning of the reactants was such as to leave little or no control over it.

Fig. 6 shows the rearrangement of the apparatus designed to

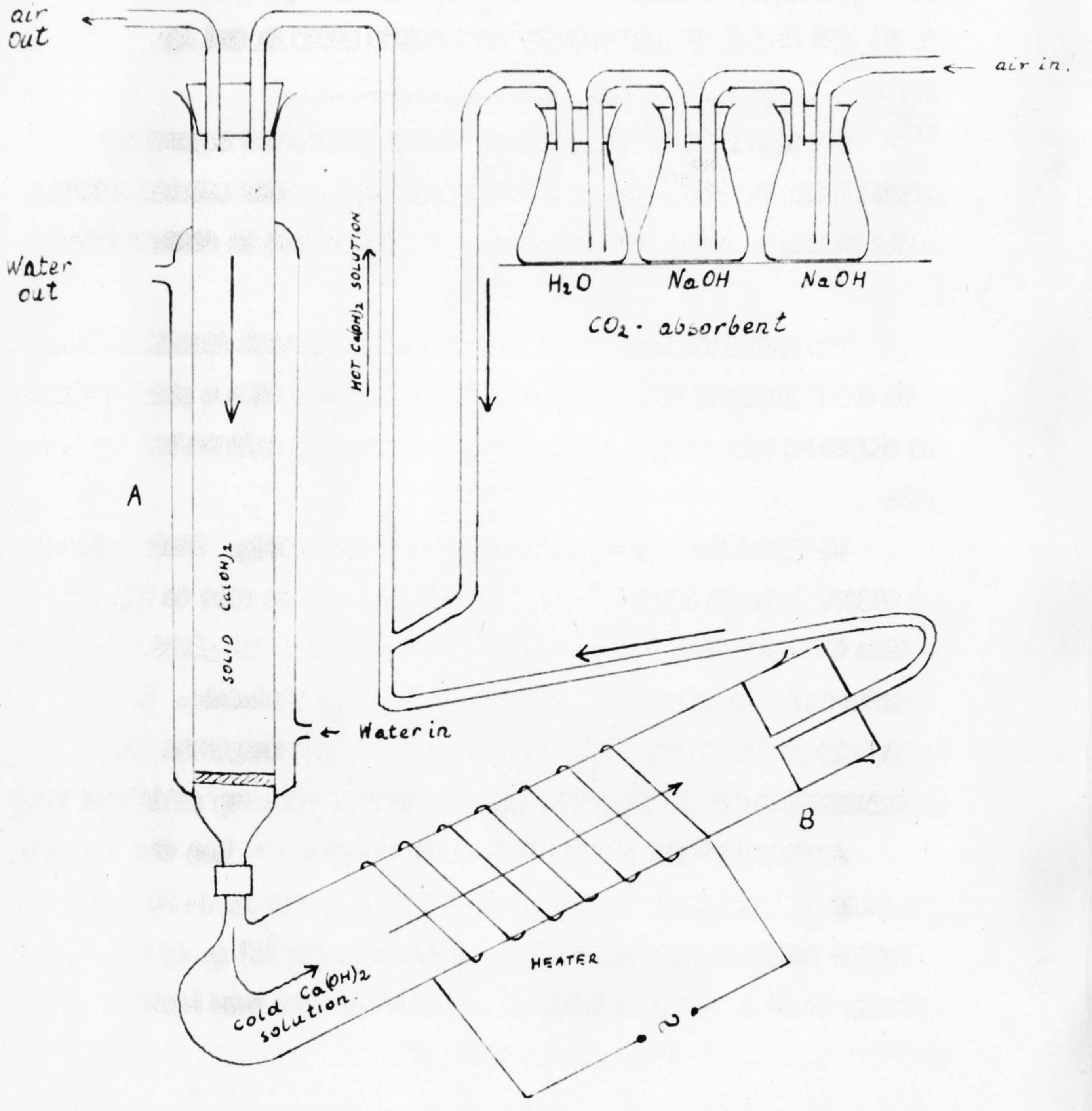

Fig. 6. Apparatus used to grow $Ca(OH)_2$ crystals from warm aqueous solution.

eliminate the disadvantages of the above procedure, notably to delay the mixing and to bring the reactants into contact in a much diluted state. The diffusion cell was made from 1/4" thick perspex plastic. The cell was divided into 3 compartments by the movable sides $S_1$ and $S_2$. F is a plastic strip put across the bottom of the portion D.

The reactants (KOH and $CaCl_2$) were placed in the separatory funnels E and F. Upon opening the stopcocks the heavier solutions fell to the bottom of A and B respectively and were allowed to diffuse into D.

The procedure followed was to fill the cell with distilled water, place the separatory funnels in position and cover C with a plastic sheet. The stopcocks were opened and the apparatus was left undisturbed for one week.

We were able to secure small crystals of $Ca(OH)_2$. Their size did not exceed 2 mm. in length. After several attempts we came to the conclusion that even this improved diffusion method does not yield large crystals suitable for nuclear magnetic resonance experiments. This appears to be due to the fact that $Ca(OH)_2$ is very susceptible to supersaturation and it deposits freely in contact with any solid surface.

Another method we have tried was based upon the fact that $Ca(OH)_2$ has a negative temperature gradient of solubility. Thus, at 100°C the saturated solution contains 0.077 g. of the base per 100 g. of solution, whereas, at 0° it contains 0.185 g. It is clear that upon heating the solution from 0°C to 100°C, we should be able to induce the deposition of 0.108 g. of $Ca(OH)_2$.

Fig. 7 shows the arrangement. Tube A cooled by a water jacket was

Fig 8. Synchronous motor shaft used in the temperature regulating device.

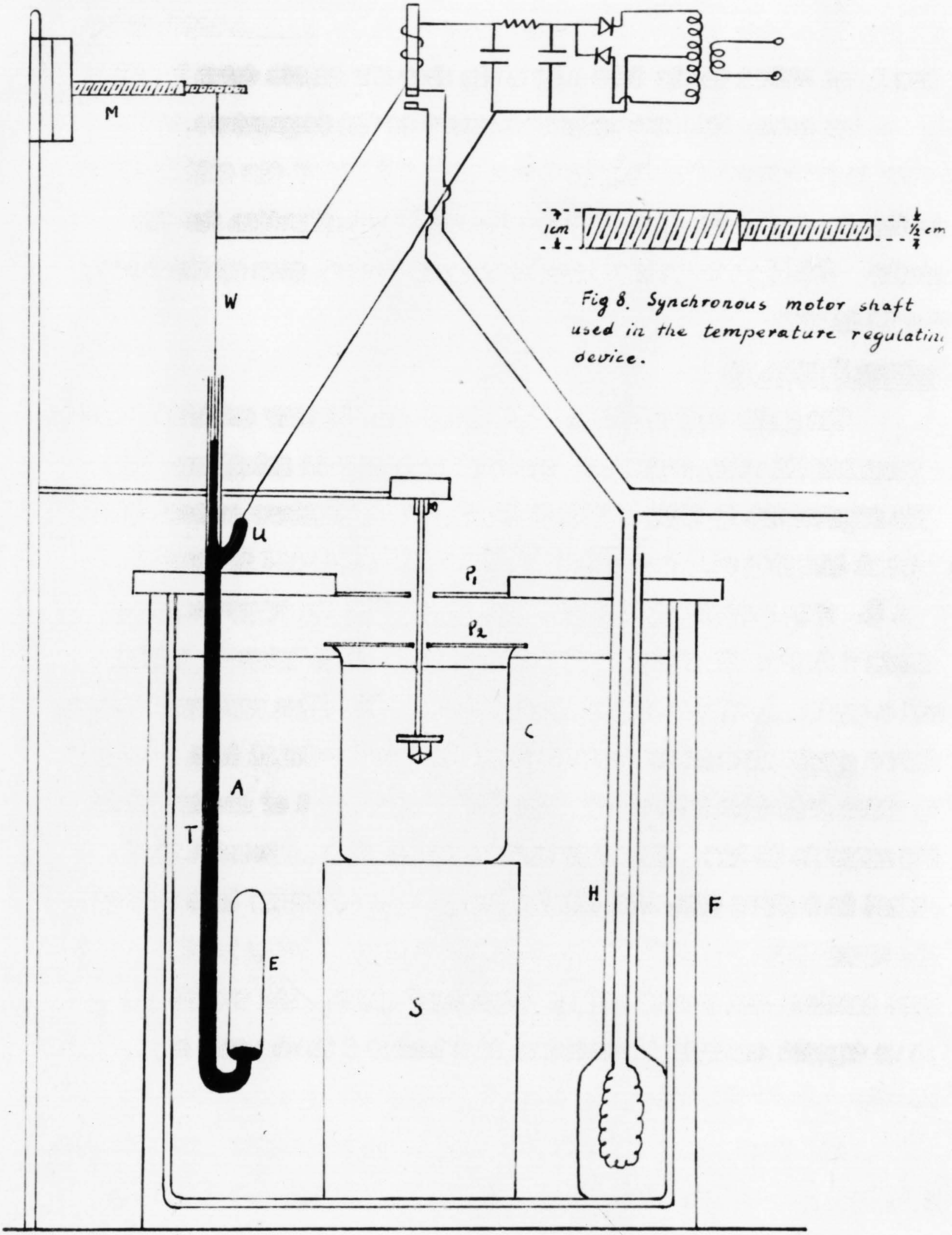

Fig 7. Water-bath used to grow primary alkali phosphates.

filled with solid $Ca(OH)_2$ supported on glass-wool pads. Tube B, slightly sloping upwards, was heated electrically. The hot solution which issued from B was lifted to the tube A by a $CO_2$ free air stream drawn by means of a water pump. In A the water was cooled to the temperature of the water jacket and as it percolated through it dissolved the solid $Ca(OH)_2$ on its way down. The apparatus was in continuous operation for two months. $Ca(OH)_2$ was obtained in the form of flakes, some of which were 9 $mm.^2$ in area.

Primary Phosphates

The primary phosphates, $MH_2PO_4.XH_2O$ are all very soluble in water. Supersaturation was produced by cooling the saturated solutions. The main requirement in this technique is a rigid temperature control and a gradual lowering of the temperature. The apparatus used is shown in Fig. 8. T is a thermostat constructed to control the temperature to within ± 0.1°C. It consists of a tube E filled with toluene, a tube A and a capillary tube G with a sidearm U, all containing mercury. Hanging from a synchronous motor shaft by means of a nylon thread is a steel wire W, which just dips into the mercury in G. The period of revolution of the motor is 24 hrs. The water bath heater H, is a nichrome-A wire sealed in a glass tube with oil for the purpose of better heat exchange. The water bath is a 16 gallon earthenware vessel, heavily insulated with wood shavings and covered with a "styrofoam" sheet. The solution which is to deposit crystals is contained in a beaker C which rests on a support S. The additional features of the beaker will be explained later.

The synchronous motor shaft, Fig. 9, consists of a 1 cm. dia. and a 1/2 cm. dia. screw. The 1/2 cm. dia. portion is used in the initial part of the experiment when the growing crystals are small. This is to ensure that the supersaturation does not reach a spontaneous nucleation level.

The description of the experimental procedure follows. The water in the tank is heated to 40°C. The salt solution is preheated to 50° and then lowered into the tank, followed by mechanical stirring for about a day. After that period the saturated solution is decanted off, preheated to 45°C, filtered and replaced in the water tank.

We have tried 3 methods of seeding the solution with small crystals. A small perfect crystal was tied to a glass rod by means of a nylon fibre and lowered into the solution. It did not give satisfactory results chiefly because the nylon fibre served as a site where the solution tended to deposit crystals. Another method tried was to drop the crystal seed to the bottom of the container. To prevent the crystals grown at the surface from falling down we inserted a glass sheet a few inches above the bottom of the container. The crystals grown were fairly large (of the order of 1") with large clear portions. The last method of attachment of the crystal seed used was to cement the crystal to the shaft of a synchronous motor (30 rpm). This method gave satisfactory results.

When the solution had been replaced in the water bath, the latter was carefully covered with a styrofoam sheet and both the synchronous motors started. The apparatus was left undisturbed until the temperature of the water bath reached that of the surroundings. The duration of the experiment ranged from two to three weeks.

Using the techniques described above we have grown nearly perfect

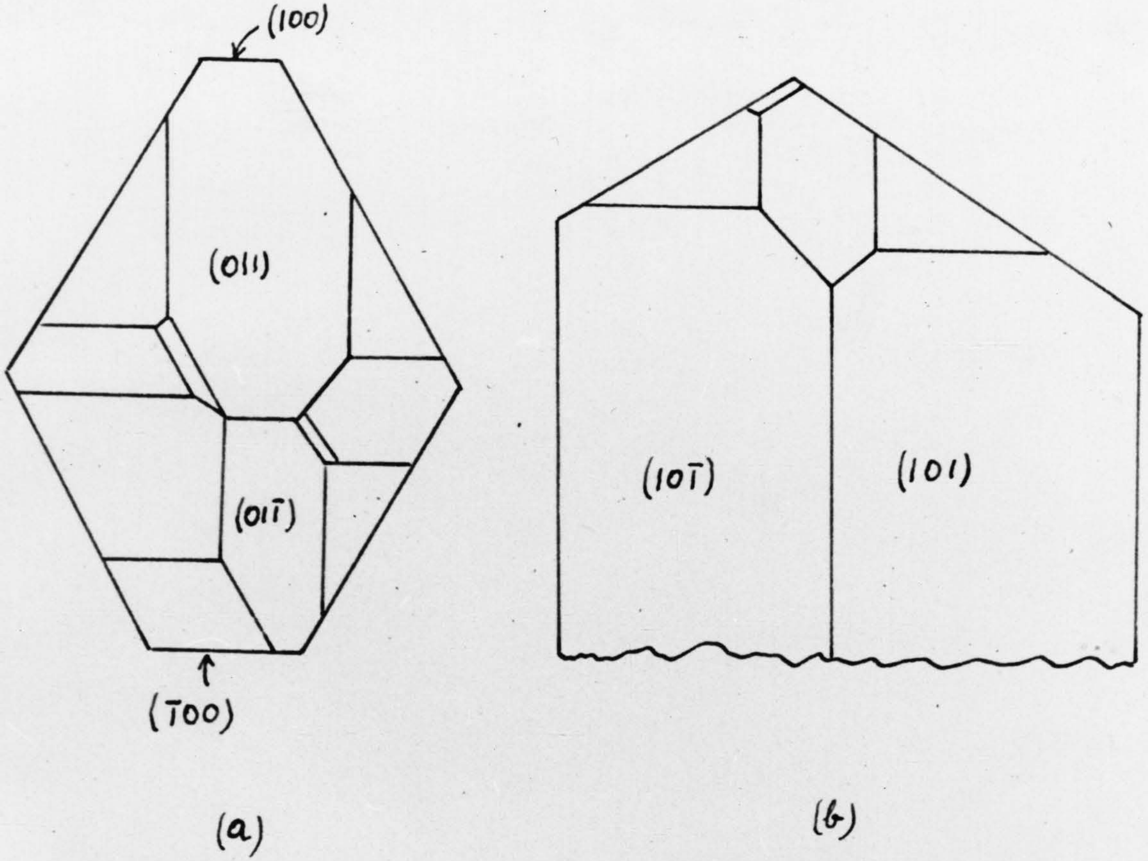

Fig 10.

Crystal habits of sodium dihydrogen phosphate dihydrate.

crystals of $NaH_2PO_4 \cdot 2H_2O$ of the order 1" to 1-1/2" in length. The crystals grown were of the form of bipyramidal sphenoids with faces $(10\bar{1})$, $(101)$, $(011)$, $(01\bar{1})$, $(100)$ and $(\bar{1}00)$ well developed. Fig. 10 (a) and (b) show a 1:2 scale drawing of one of the crystals. These crystal faces were used to locate the crystallographic axes.

## II. INTRODUCTION

This section of the thesis describes the experimental observation of the complete radio-frequency resonance absorption spectrum of $Na^{23}$ nuclei in a single crystal of $NaH_2PO_4.2H_2O$ placed in a homogeneous external magnetic field $H_o$ of approximately 5080 gauss. The theoretical interpretation of this spectrum in terms of the electrostatic interaction between the $Na^{23}$ nuclei and their surroundings in the crystal is also presented. The detailed study of the effects on the magnetic resonance absorption spectrum of the nuclear electric quadrupole moment interaction with its surroundings in single crystals will be outlined. Such a study can yield useful information about the nuclear spin and the ratios of quadrupole moments of isotopes on one hand and about the properties of the crystal symmetry and electric field gradients existing of nuclear sites on the other.

A nuclear magnetic resonance spectrum arises from the fact that a nucleus of spin I and magnetic moment $\mu$ placed in a uniform magnetic field $H_o$ has 2I + 1 equidistant Zeeman energy levels. A weak linearly polarized oscillating magnetic field perpendicular to $H_o$, of frequency $\nu_o = \frac{uH_o}{Ih}$ will induce transitions between adjacent levels. In a sample containing many identical nuclei which do not interact with one another but do interact with $H_o$, the energy levels will be the same for all the nuclei. If the nuclear spins are in thermal equilibrium with their surroundings, the lower energy states will be more heavily populated with the result that the induced transitions between the adjacent energy levels will give a net absorption of energy by the sample at the single resonant frequency $\nu_o$. With $H_o$ in the neighbourhood of 10000 gauss, this frequency lies in the radio-frequency range for most nuclei, so that radio-frequency techniques can be employed. For $Na^{23}$ at 5080 gauss $\nu_o$ occurs at 6.538 Mc./Sec.

If the nucleus has a non-zero electric quadrupole moment Q, this moment can interact with the inhomogeneous electric field if such exists at the nuclear sites in a crystal. In a single crystal in which there is only one type of site for a particular element, there will be a large number of similarly situated nuclei which are all subjected to the same kind of an inhomogeneous electric field, which repeats itself periodically from unit cell to unit cell. Under these conditions some or all of the 2I + 1 Zeeman levels of the nucleus are perturbed and are no longer equidistant, with the result that the 2I transitions between the adjacent levels are no longer of the same frequency but give rise to a spectrum of 2I lines. The original work in this field was carried out by Pound (4) who studied the $Al^{27}$ spectrum in $Al_2O_3$, which is a special case because of the uniaxial nature of $Al_2O_3$. A group of experimenters at the University of British Columbia extended Pound's theory to cover the general case and carried out experimental studies of the $Li^7$ (1) and $Al^{27}$ (2) spectra in spodumene, $Li\ Al\ (Si)_3)_2$ . Watermann and Volkoff (3) and Eades (11) have recently studied the $B^{11}$ and $Na^{23}$ spectra in kernite $(Na_2B_4)_7.4H_2O)$ and euclase.

As a preliminary to studying the effect of temperature on the degree of ionicity of chemical bonds in crystals the electric field gradients at the Na sites in $NaH_2PO_4.2H_2O$ have been completely determined for the crystal of room temperature.

# CHAPTER I

## THEORY

This chapter outlines the theory of the dependence of the nuclear magnetic resonance frequencies in a single crystal on the orientation of the crystal with respect to a uniform magnetic field $H_o$. The general case has been discussed by Pound (4), Bersohn (5) and Volkoff (6). This discussion will be limited to the case when the interaction of the nuclear quadrupole moment eQ, with the electric field gradient $\Delta E = -\Delta^2 \phi$ in a crystal is small compared to the interaction between the nuclear magnetic dipole moment u and $H_o$ but large compared to the nuclear dipole-dipole interactions.

### Perturbation Theory

Following the authors of the references (4), (5) and (6) the Hamiltonian for nuclei exposed simultaneously to a uniform magnetic field $H_o$ and an electric field gradient $\Delta E$ is given by:

$$H = -\mu . H_o + F$$

and $F = Q . \Delta E$ is the interaction of the electric field gradient $\Delta E$ with the nuclear electric quadrupole tensor Q as discussed by Pound (4). F is treated as a small perturbation. The influence of F on the unperturbed Zeeman energy levels $E^o m$ may be expressed in terms of the matrix elements of F in the representation diagonalising the magnetic energy operator:

$$E_m = E^0_m + F_{mm} + \sum_{m'} \frac{F_{mm'} F_{m'm}}{E^0_m - E^0_{m'}}$$

In the notation of Ref. 7

$$F_{m,m^1} = \langle \alpha, m | F | \alpha, m^1 \rangle$$

where m and $m^1$ are the magnetic quantum numbers in which the nucleus finds itself. $\Delta E$ is entirely independent of the state of the nucleus, therefore

$$F_{m,m^1} = \alpha m \; Q_q \; \alpha m^1 \quad \Delta E_q$$

where q takes the values $0, \pm 1, \pm 2$.

The explicit relations are:

$$F_{m,m} = \langle \alpha m | Q_0 | \alpha m \rangle = \frac{eQ}{I(2I+1)} \left[3m^2 - I(I+1)\right] \quad \ldots\ldots\ldots 2a$$

$$F_{m,m\pm1} = \langle \alpha m | Q_{\pm1} | \alpha m\pm1 \rangle = \sqrt{\frac{3}{2}} \frac{eQ}{I(2I+1)} (2m\pm1) \sqrt{(I\mp m)(I\pm m+1)} \quad \ldots 2b$$

$$\begin{aligned} F_{m,m\pm2} &= \langle \alpha m | Q_{\pm2} | \alpha m\pm2 \rangle \\ &= \sqrt{\frac{3}{2}} \frac{eQ}{I(2I+1)} \sqrt{(I\mp m)(I\pm m+1)(I\mp m-1)(I\pm m+2)} \quad \ldots\ldots 2c \end{aligned}$$

Substituting (2) in (1) leads to the energy relations in the form given by Bersohn (3):

$$\begin{aligned} E_m = &-m \frac{\mu}{I} H_0 + \frac{eQ}{2I(2I-1)} \left[3m^2 - I(I+1)\right] (\Delta E)'_0 \\ &+ \frac{3(eQ)^2}{4I^2(2I-1)^2} \frac{m}{(\mu/I) H_0} \left\{ \left|(\Delta E)_{\pm1}\right|^2 \left[4I(I+1) - 1 - 8m^2\right] \right. \\ &\left. - \left|(\Delta E)'_{\pm2}\right|^2 \left[2I(I+1) - 1 - 2m^2\right] \right\} \end{aligned}$$

+ third order terms. . . . . . . . . . . . . . 3

The frequency corresponding to transitions between adjacent energy levels is given by:

$$\nu_{m \leftrightarrow m-1} = \left| \frac{E_m - E_{m-1}}{h} \right|$$

For nuclei with $I = 3/2$ there are four available energy levels which give rise to three possible transition frequencies which we denote by $\nu_c$, $\nu'$, $\nu''$ where $\nu_c$ denotes the "central" line corresponding to the two transitions $m = \pm 1/2 \leftrightarrow \mp 1/2$. Since there is no way of determining which line corresponds to $m = +3/2 \leftrightarrow +1/2$ and which to $m = -3/2 \leftrightarrow -1/2$, either one is denoted by $\nu'$ and the other by $\nu''$.

$$\text{Putting } C_z = \frac{eQ\phi_{zz}}{h} \quad \ldots\ldots 4$$

where $\phi_{zz}$ is defined at the end of the chapter, we get:

$$\nu' - \nu'' = 2 C_z \frac{(\Delta E)'_0}{\phi_{zz}} + \text{third order terms} \quad \ldots\ldots\ldots\ldots 6$$

$$\nu_c - \nu_0 = \frac{C_z^2}{\nu_0} \left[ \frac{1}{2} \left| \frac{(\Delta E)'_{\pm 1}}{\phi_{zz}} \right|^2 - \left| \frac{(\Delta E)'_{\pm 2}}{\phi_{zz}} \right|^2 \right] + \text{fourth order terms} \quad \ldots 7$$

$$\frac{\nu' + \nu''}{2} - \nu_0 = \frac{C_z^2}{\nu_0} \left| \frac{(\Delta E)'_{\pm 1}}{\phi_{zz}} \right|^2 + \text{fourth order terms} \quad \ldots\ldots\ldots\ldots 8$$

## Rotation of Crystal

$\Delta E$ expressed in the laboratory Cartesian co-ordinate system (x', y', z') appears as follows:

$$(\Delta E)'_0 = -\frac{1}{2} \frac{\partial E_{z'}}{\partial z'} \equiv -\frac{1}{2} \phi_{z'z'} \quad \ldots\ldots\ldots\ldots\ldots 9$$

$$(\Delta E)'_{\pm 1} = \pm \frac{\sqrt{6}}{6} \left[ \frac{\partial E_{x'}}{\partial z'} \pm i \frac{\partial E_{y'}}{\partial z'} \right] \equiv \pm \frac{\sqrt{6}}{6} \left[ \phi_{x'z'} \pm i \phi_{y'z'} \right] \quad \ldots\ldots 10$$

$$(\Delta E)'_{\pm 2} = -\frac{\sqrt{6}}{12} \left[ \frac{\partial E_{x'}}{\partial x'} - \frac{\partial E_{y'}}{\partial y'} \pm 2i \frac{\partial E_{x'}}{\partial y'} \right] \equiv -\frac{\sqrt{6}}{12} \left[ \phi_{x'x'} - \phi_{y'y'} \pm 2i \phi_{x'y'} \right] \quad \ldots 11$$

We introduce another system of co-ordinates (X, Y, Z) fixed with respect to the crystallographic axes and about each of which the crystal is rotated with respect to the external magnetic field in a laboratory co-ordinate system in which the magnetic field defines the direction of z'. The tensor components in the laboratory system (x', y', z') are related to those in the (X, Y, Z) co-ordinate system which is fixed in the crystal, by the transformation law:

$$\phi_{q'_i q'_j} = \sum_{\alpha,\beta} \phi_{Q_\alpha Q_\beta} \frac{\partial Q^\alpha}{\partial q'_i} \frac{\partial Q^\beta}{\partial q'_j}$$

Where Q refers to the (X, Y, Z) system while q' refers to the (x', y', z') system; $\alpha$ and $\beta$ as well as i and j take values 1, 2, 3; $\phi_{q'_i q'_j}$ are the tensor components in (x', y', z') while $\phi_{Q_\alpha Q_\beta}$ are the tensor components in the (X, Y, Z) system. Using 12 and 9 we get:

$$(\Delta E)'_0 = \frac{1}{4}(\Phi_{yy} + \Phi_{zz}) + \frac{1}{4}(\Phi_{yy} - \Phi_{zz})\cos 2\theta_x - \frac{1}{2}\Phi_{yz}\sin 2\theta_x \quad \ldots 13$$

In the derivation of 13 we used the relation:

$$X = y'$$
$$Y = \cos(\theta\ x)z' + \sin(\theta\ x)x'$$
$$Z = -\sin(\theta\ x)z' + \cos(\theta\ x)x' \quad \ldots\ldots 14$$

Applying (12) on (14) for the case of (10) and (11) one gets:

$$(\Delta E)_{\pm 1} = \frac{\sqrt{6}}{6}\left\{\mp\left[\Phi_{yz}\cos 2\theta_x + \frac{1}{2}(\Phi_{yy} - \Phi_{zz})\sin 2\theta_x\right] - i\left[\Phi_{xy}\cos\theta_x - \Phi_{zx}\sin\theta_x\right]\right\} \quad \ldots\ldots 15$$

$$(\Delta E)_{\pm 2} = \frac{\sqrt{6}}{12}\left[\frac{3}{2}(\Phi_{yy} + \Phi_{zz}) - \frac{1}{2}(\Phi_{yy} - \Phi_{zz})\cos 2\theta_x + \Phi_{yz}\sin 2\theta_x \pm 2i(\Phi_{zx}\cos\theta_x + \Phi_{xy}\sin\theta_x)\right] \quad \ldots 16$$

The expressions (13), (15) and (16) when substituted into (6) and (7) yield an explicit expression of the dependence of the separation of the "satellites" $(\nu' - \nu'')$ and of the "centre of gravity" of the satellites $\frac{\nu'' + \nu''}{2}$ on the angle of rotation $\theta_x$. In the first case the expression assumes the following form:

$$(\nu' - \nu'')_x = a_x + b_x\cos 2\theta_x + c_x\sin 2\theta_x \quad \ldots\ldots 17$$

and in the second case the expression becomes:

$$\frac{\nu' + \nu''}{2} - \nu_0 = n_x + p_x\cos 2\theta_x + r_x\sin 2\theta_x + u_x\cos 4\theta_x + v_x\sin 4\theta_x \ldots 18$$

The coefficients in (17) and (18) are related to the electrostatic field gradient tensor components as follows:

$$a_x = \frac{C_z}{2\Phi_{zz}}(\Phi_{yy} + \Phi_{zz}) \quad \ldots\ldots 19$$

$$b_x = \frac{C_z}{2\Phi_{zz}}(\Phi_{yy} - \Phi_{zz}) \quad \ldots\ldots 20$$

$$c_x = -\frac{C_z}{\Phi_{zz}}\Phi_{zy} \quad \ldots\ldots 21$$

$$n_x = \frac{1}{12\nu_0}(b_x^2 + c_x^2 + c_y^2 + c_z^2) \quad \ldots\ldots 22$$

$$p_x = \frac{1}{12\nu_0}\left(c_y^2 - c_z^2\right) \quad \ldots\ldots\ldots\ldots \quad 23$$

$$r_x = -\frac{1}{6\nu_0}\left(c_y c_z\right) \quad \ldots\ldots\ldots\ldots \quad 24$$

$$u_x = -\frac{1}{12\nu_0}\left(b_x^2 - c_x^2\right) \quad \ldots\ldots\ldots\ldots \quad 25$$

$$v_x = -\frac{1}{6\nu_0}\left(b_x c_x\right) \quad \ldots\ldots\ldots\ldots \quad 26$$

By a suitable method of analysis of the experimental data, the numerical values of the tensor components $\frac{C_z}{\phi_{zz}} \phi_{ij} \equiv \psi_{ij}$ can be determined. The tensor can be diagonalised in the usual way and a set of 3 principal values (eigenvalues) can be obtained. Diagonalisation involves the solution of the cubic equation:

$$\gamma^3 - a\gamma - b = 0 \quad \ldots\ldots\ldots\ldots\ldots\ldots \quad 27$$

where:

$$a = \frac{C_z^2}{\phi_{zz}^2}\left(\phi_{xy}^2 + \phi_{yz}^2 + \phi_{zx}^2 - \phi_{xx}\phi_{yy} - \phi_{yy}\phi_{zz} - \phi_{zz}\phi_{xx}\right) \ldots \quad 27a$$

and

$$b = \frac{C_z^3}{\phi_{zz}^3}\left(\phi_{xx}\phi_{yy}\phi_{zz} + 2\phi_{xy}\phi_{yz}\phi_{zx} - \phi_{xx}\phi_{yz}^2 - \phi_{yy}\phi_{zx}^2 - \phi_{zz}\phi_{zy}^2\right) \ldots \quad 27b$$

27 yields 3 roots $\gamma_1$, $\gamma_2$, $\gamma_3$ given by:

$$\gamma_n = 2\left(\frac{a}{3}\right)^{\frac{1}{2}} \cos\left[\alpha - \frac{2\pi n}{3}\right]$$

where, $\cos 3\alpha = \frac{|b|}{2}\left(\frac{3}{a}\right)^{\frac{3}{2}}$

$\gamma_3$ has largest absolute value and is positive while $\gamma_1$ and $\gamma_2$ have smaller absolute values and are both negative.

From this we also get the asymmetry parameter defined as:

$$\eta = \frac{\gamma_1 - \gamma_2}{\gamma_3} = \frac{\phi_{xx} - \phi_{yy}}{\phi_{zz}}$$

$\gamma_3$ is also called the "quadrupole coupling constant":

$$\gamma_3 = C_z = \left|\frac{eQ\phi_{zz}}{h}\right|$$

The axes (x, y, z) refer to the principal axes of the tensor $\phi_{ij}$.

The process of diagonalisation also gives the direction cosines of the axes (x, y, z) with respect to (X, Y, Z). Denoting the direction cosines by $\lambda_n$, $\mu_n$, $\nu_n$ we get:

$$\frac{\lambda_n}{D_{1n}} = \frac{\mu_n}{D_{2n}} = \frac{\nu_n}{D_{3n}} = \frac{\pm 1}{D_{1n}^2 + D_{2n}^2 + D_{3n}^2} \qquad \ldots\ldots\ldots\; 32$$

where

$$\left.\begin{aligned} D_{1n} &= \Psi_{xy}\Psi_{yz} - \Psi_{zx}(\Psi_{yy} - \gamma_n) \\ D_{2n} &= \Psi_{xz}\Psi_{xy} - \Psi_{yz}(\Psi_{xx} - \gamma_n \\ D_{3n} &= (\Psi_{yy} - \gamma_n)(\Psi_{xx} - \gamma_n) - \Psi_{xy}^2 \end{aligned}\right\} \qquad \ldots\ldots\ldots\; 33$$

The steps in the analysis of the experimental results will therefore be as follows:

1) The curves of the forms of Equations (17) and (18) are fitted to the experimentally observed frequencies and yield experimental values of the Fourrier coefficients.

2) These experimental Fourrier coefficients are then used in Equations (19) to (26) to obtain the components of the tensor $\Psi_{ij}$ in X, Y, Z co-ordinate system.

3) This tensor is then diagonalised using Equations (27) to (29). The direction cosines are also evaluated using (32) and (33).

The theory outlined in this chapter will be used in the experimental part of this section, namely, in chapters III and IV.

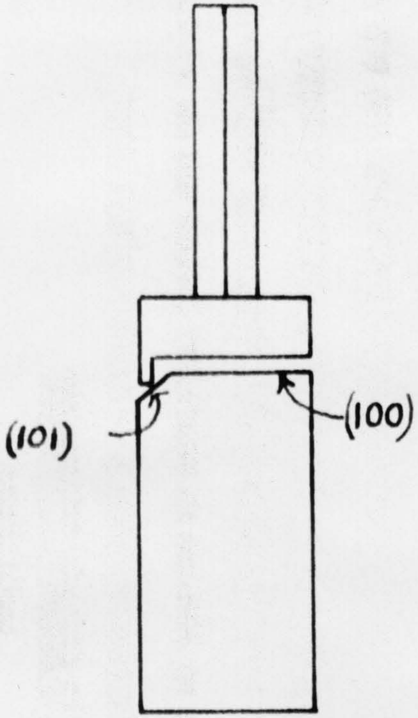

Fig 11

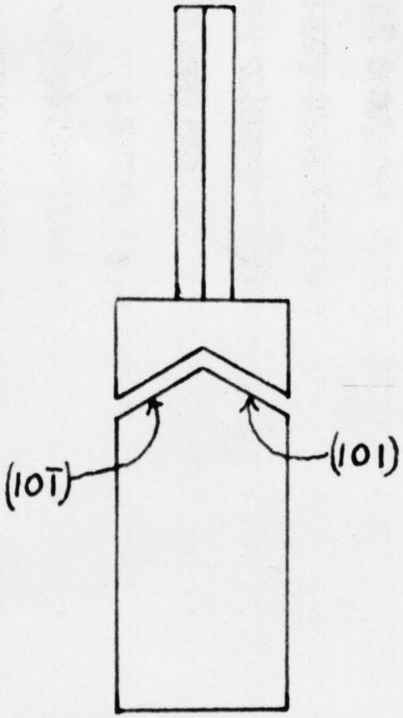

Fig. 12

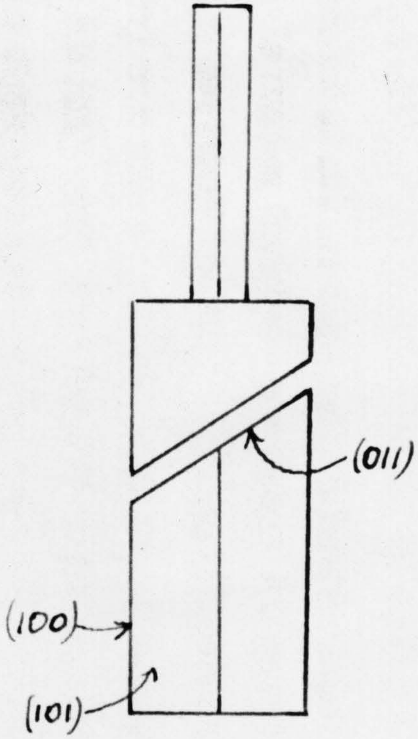

Fig 13

Attachment of crystal sections used for Z-, X- and Y-rotations.

# CHAPTER II

## EXPERIMENTAL PROCEDURE

Large single crystals of $NaH_2PO_4.2H_2O$ were grown from an aqueous solution by the method discussed in Chapter II of Section I. These crystals were grown under the correct temperature range so that the crystalline substance obtained was in the form of $NaH_2PO_4.2H_2O$ crystals and not the corresponding monohydrate which is also possible to get from aqueous solution. $NaH_2PO_4.2H_2O$ crystals are known to belong to the orthorhombic system and have the $P_{222}$ space groups. Other than the space group, little seems to be known about their structure.

A number of $NaH_2PO_4.2H_2O$ crystals were grown and some of the poorer ones were used for a preliminary study of $Na^{23}$ resonance lines. For the final experiments two particularly good crystals were chosen. These were checked using polarized light to make sure that they were not twinned or badly strained. One of these crystals was about 1" x 1" x 1/2" in size and had a particularly well developed (001) face. It was ground roughly to a cylindrical shape of 1/2" dia., the axis of the cylinder perpendicular to the (001) face, i.e., parallel to the "c" crystallographic axis. The (001) face and the edges defining the intersection between the faces (001) and (101), and $(10\bar{1})$ respectively, were carefully preserved during the process of grinding. The crystal was then glued to a lucite mount as shown in Fig. 11. The edges served to define the angular orientation, while the face (001) served to fix the axis of rotation.

The pieces of crystal used for the X and Y rotation were cut from the same large crystal whose dimensions were 1" x 1" x 1-1/2". This crystal had $(101)$, $(10\bar{1})$, $(011)$ and $(01\bar{1})$ faces very well developed. The first cylinder was ground with its axis parallel to the "a" crystallographic axis with the faces $(101)$ and $(10\bar{1})$ and the edge between them carefully preserved during the process of grinding. A lucite mount was then machined with a wedge of 119° 45' such that the rotation axis was along the bisector of this angle. When the crystal was glued in the position shown in Fig. 12, the shape of the mount assured that the "a" axis would be parallel to the rotation axis. The edge defining the intersection between the $(101)$ and $(10\bar{1})$ faces is parallel to the "b" axis and was used for angular orientation.

The piece of the crystal used for the Y rotation was also cut in the shape of a cylinder with $(011)$ carefully preserved during grinding. The $(011)$ face was then glued to a mount which had been machined at an angle of 57° 45' so that the "b" axis was parallel to the rotation axis. Fig. 13 shows the arrangement.

Each of the three crystals was wrapped tightly with "Saran" plastic to prevent exposure to the atmosphere as it had been found during the preliminary work that the crystal dehydrated very rapidly upon prolonged contact with dry air. The lucite mounts described above were in turn locked in position in an angle-measuring device inside the gap between the magnet poles.

The angle-measuring device consisted of a stainless steel (non-magnetic) block, which could be adjusted by a set of screws to fit the gap between the magnet poles tightly, and a calibrated dial assembly. The lucite crystal mounts were held rigidly by the calibrated dial assembly which would rotate in the stainless steel block, with the axis of rotation always held perpendicular to the magnetic field. The dial was calibrated at one degree intervals and, with the aid of a magnifying glass, relative measurements could be repeated consistently to better than half a degree.

Rotations about the a, b, c crystallographic axes, which will be referred to as the rotations about the X, Y, Z axes respectively, were made at 30° intervals in the intervals 0° - 180° and 195° - 345°. The apparatus used to record the signals has been adequately described in the thesis by K. A. Lines (9). The only modification introduced was that the sample coil and the modulating coils were detached from the oscillating detector chassis and fixed inside the gap between the magnet poles. Electrical connections were made using a coaxial cable. This arrangement greatly facilitated the experiment, especially the alignment of the crystal.

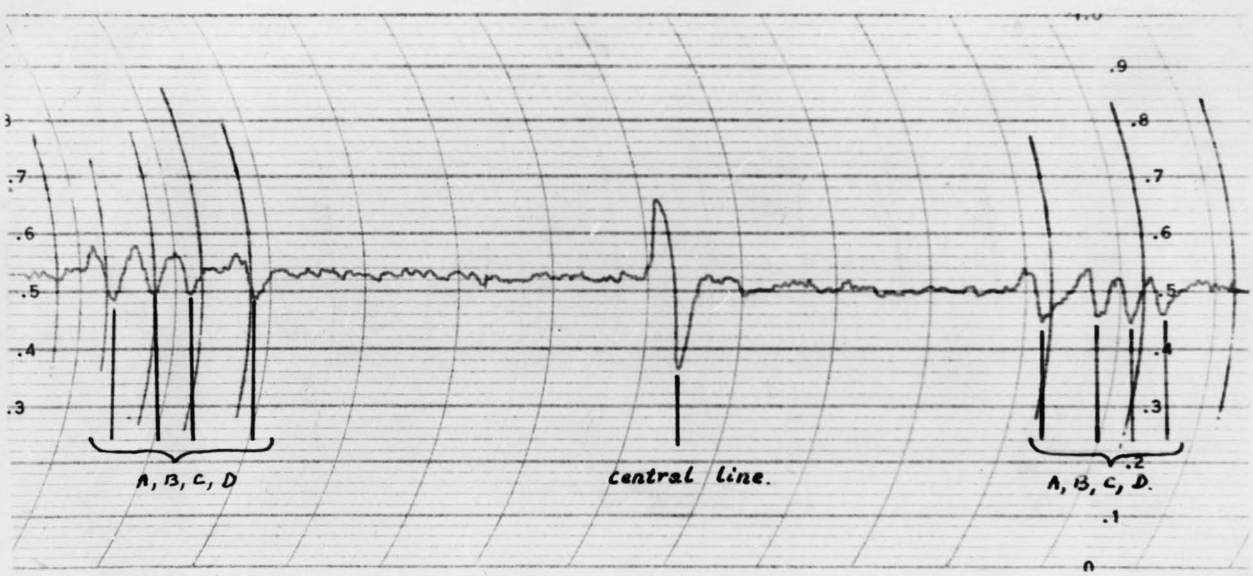

Fig 14 a Chart recording of the $Na^{23}$ spectrum at $\theta_x = 90°$. The "a" crystallographic axis is at a small angle to the rotation axis.

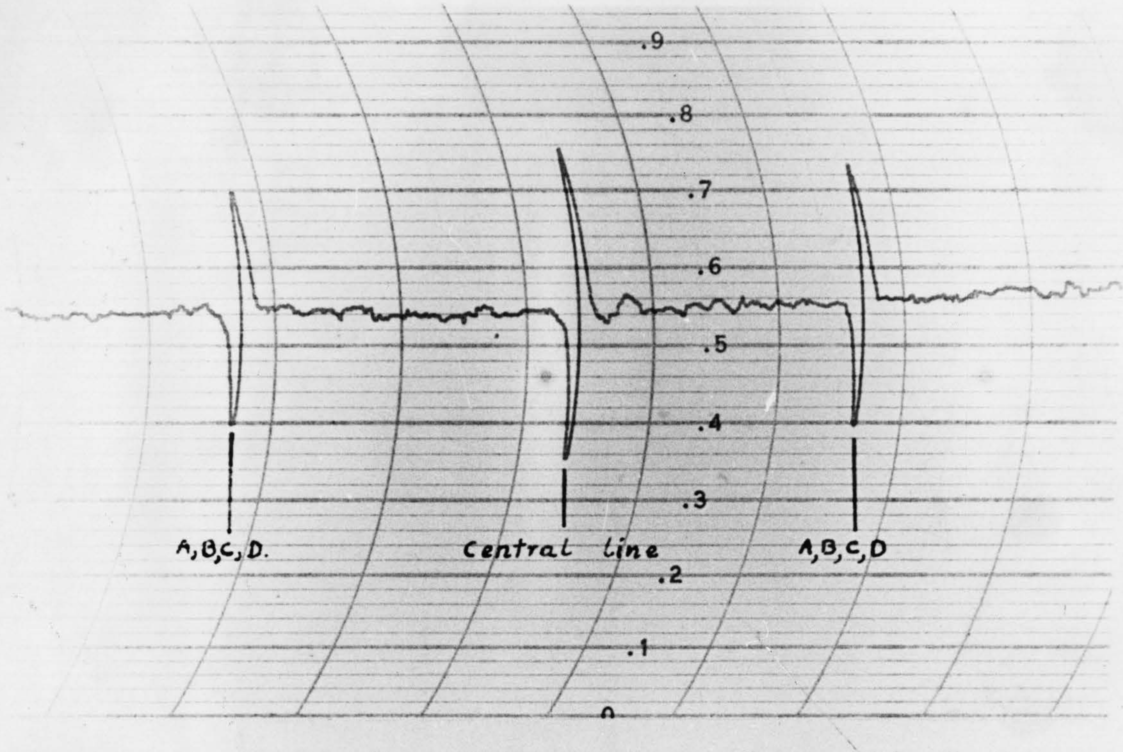

Fig. 14 b. Chart recording of the spectrum at $\Theta_x = 90°$. The "a" crystallographic axis is along the rotation axis.

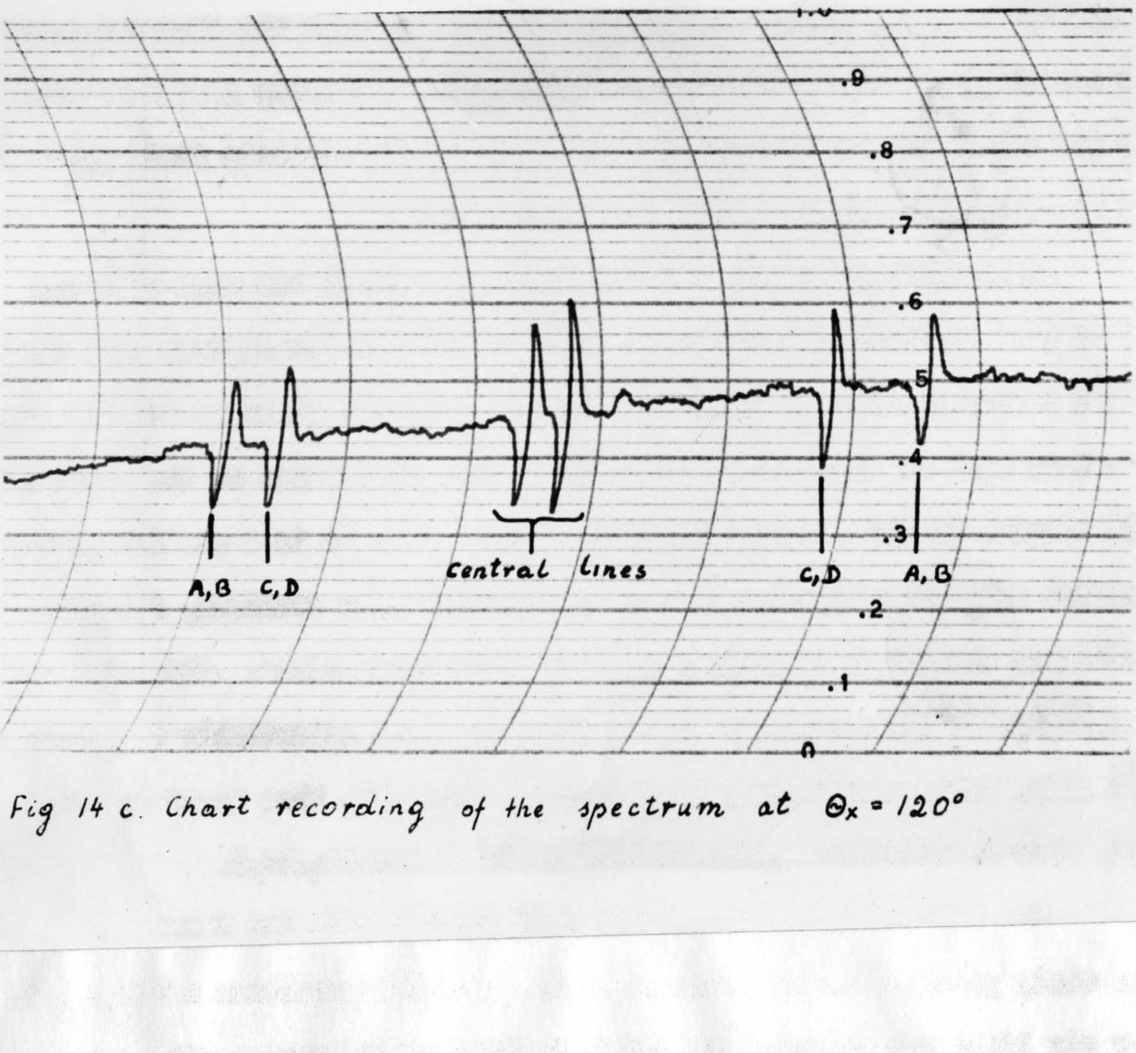

Fig 14 c. Chart recording of the spectrum at $\Theta_x = 120°$

# CHAPTER III

## EXPERIMENTAL RESULTS AND CALCULATIONS

The nuclear magnetic resonance spectrum of $Na^{23}$ was studied in a single crystal of $NaH_2PO_4.2H_2O$. The complex spectrum obtained has been analysed using the theory outlined in Chapter I. From the data obtained the electric quadrupole coupling constants, the asymmetry parameters and the direction cosines of the principal axes of the electric field gradient tensor have been calculated for the sodium sites.

A preliminary study of a $NaH_2PO_4.2H_2O$ crystal was made with the X axis ("a" crystallographic axis) at an angle of a few degrees with respect to the rotation axis. A maximum of twelve lines was observed and the frequency of each of these lines depended on the orientation of the crystal with respect to the external magnetic field. Fig. 14a is a section of the recorder chart showing nine lines. The central line consists, for this particular crystal orientation, of four overlapping lines. Since the spin of $Na^{23}$ is $I = 3/2$ we expect $2I = 3$ lines for each essentially different $Na^{23}$ site. This preliminary investigation indicates that there are at most, four essentially different $Na^{23}$ sites in $NaH_2PO_4.2H_2O$.

The next step was to use the good crystal with its X axis accurately parallel to the rotation axis. For this rotation a maximum of only six lines was observed for which $O_x$ (the angle between the Y axis and the magnetic field $H_o$) was not equal to 0, 90° and 180° and when $O_x$ was equal to these angles only three lines were found. Fig. 14a can be compared to Fig. 14b for which the crystal has the same orientation except that the X axis for Fig. 14a is slightly tilted with respect to the rotation axis. It is clear that in the case of Fig. 14a (i.e. for $\theta_x = 90^\circ$) each of the two outer lines is actually composed of four overlapping unresolved lines. It is also known from the spectra obtained at other orientations (not shown) of the tilted crystal that the central line is also composed of four unresolved lines.

At this point, it is possible to carry out a fairly complete qualitative interpretation of the results obtained so far. Since $I = 3/2$ for $Na^{23}$, there should be three lines for a particular $Na^{23}$ site. The spectrum obtained, however, is more complex and consists of twelve lines. The rest of the analysis is based on the assumption that the sodium nuclei occupy a number of sites whose electric field gradients differ at least in some respect, and that the "complex" spectrum is due to the superposition of the expected "simple" spectra due to each set of nuclei*. Since the maximum number of lines observed was twelve and each "simple" spectrum for $Na^{23}$ should consist of three lines, it is apparent that for $Na^{23}$ there must be at least four sites in $NaH_2PO_4.2H_2O$ with their electric field gradient differing in some respect. Now in the X rotation never more than six lines appear. We interpret these facts using the knowledge (3) that if two sites are related by a two-fold rotation axis, the electric field gradient tensors at the two sites must have identical eigenvalues and differ only in the orientation of their principal axes, although they must be symmetrically inclined with respect to the dyad axis. Then, if

---

*The electric field gradients at these sites may differ in either the numerical values of the field gradient tensor components, the orientation of the principal axes of this tensor or both in numerical value and orientation.

# TABLE I

## The Position of the Lines of the Spectrum in Mc./Sec. for Various Orientations of the Crystal

| θ Rotation | 0° | 15° | 30° | 45° | 60° | 75° | 90° | 105° | 120° | 135° | 150° | 165° |
|---|---|---|---|---|---|---|---|---|---|---|---|---|
| X | 6.997 | 7.028 | 6.979 | 6.861 | 6.697 | 6.697 | 6.665 | 6.697 | 6.699 | 6.857 | 6.978 | 7.027 |
|  | --- | 6.891 | 6.734 | 6.565 | 6.650 | 6.559 | --- | 6.560 | 6.650 | 6.562 | 6.730 | 6.889 |
|  | 6.104 | 6.215 | 6.376 | 6.534 | 6.437 | 6.537 | 6.418 | 6.534 | 6.438 | 6.537 | 6.379 | 6.220 |
|  | --- | 6.068 | 6.123 | 6.246 | 6.408 | 6.380 | --- | 6.381 | 6.407 | 6.252 | 6.123 | 6.068 |
| Y | 6.664 | 6.700 | 6.754 | 6.809 | 6.856 | 6.879 | 6.871 | 6.878 | 6.856 | 6.812 | 6.757 | 6.702 |
|  | --- | 6.656 | 6.676 | 6.722 | 6.781 | 6.833 | --- | 6.834 | 6.782 | 6.724 | 6.679 | 6.656 |
|  | 6.416 | 6.430 | 6.414 | 6.377 | 6.323 | 6.268 | 6.228 | 6.267 | 6.319 | 6.373 | 6.415 | 6.429 |
|  | --- | 6.379 | 6.325 | 6.269 | 6.229 | 6.211 | --- | 6.211 | 6.227 | 6.269 | 6.322 | 6.375 |
| Z | 6.867 | 6.964 | 6.939 | 6.929 | 7.061 | 7.083 | 6.994 | 7.090 | 7.066 | 6.926 | 6.938 | 6.963 |
|  | --- | 6.673 | 6.711 | 6.797 | 6.579 | 6.801 | --- | 6.798 | 6.576 | 6.804 | 6.702 | 6.673 |
|  | 6.227 | 6.443 | 6.446 | 6.305 | 6.549 | 6.318 | --- | 6.318 | 6.545 | 6.298 | 6.420 | 6.443 |
|  | --- | 6.108 | 6.443 | 6.178 | 6.017 | 5.987 | 6.102 | 5.988 | 6.017 | 6.181 | 6.139 | 6.114 |

the two-fold axis is held either perpendicular or parallel to the magnetic field, the two symmetrically inclined tensors are equivalent from the point of view of the perturbation they cause and the complex spectrum will consist of only 2I transitions. It is immediately obvious that the X axis is parallel to a dyad axis. For an arbitrary orientation of the X rotation there are, in effect, only two non-equivalent sites leading to six lines. However, we have seen that at the orientation for which $\theta_X = 0^\circ$, $90^\circ$ or $180^\circ$, there are only 3 lines. Following the same reasoning as above, it is apparent that either a dyad axis is parallel to the Y axis, or to the Z axis or that there is a dyad axis parallel to each of them. It is known that two mutually perpendicular dyad axes which meet at a point have the same point group symmetry as three mutually perpendicular dyad axes meeting at the point. We can conclude, therefore, that there is a dyad axis parallel to each of the X, Y Z axes and that the electric field gradient tensors at the four sites have identical eigenvalues and differ only in the orientation of their principal axes.

In order to obtain a quantitative measurement of the eigenvalues and the orientations of each of the tensors it is necessary to carry out a complete mathematical analysis of the spectra obtained for the three rotations. Table I gives the frequencies of the satellites, i.e., the frequencies corresponding to the transitions $m = \pm 3/2 \leftrightarrow \pm 1/2$*, for various orientations of the X, Y, Z rotations. It should be pointed out that the results obtained for Y and Z rotations confirm the conclusions already drawn from the X rotation. The results tabulated in Table I are plotted

---

*The original distinction between $\nu'$ and $\nu''$ was made in a purely arbitrary manner but the data were then treated consistently.

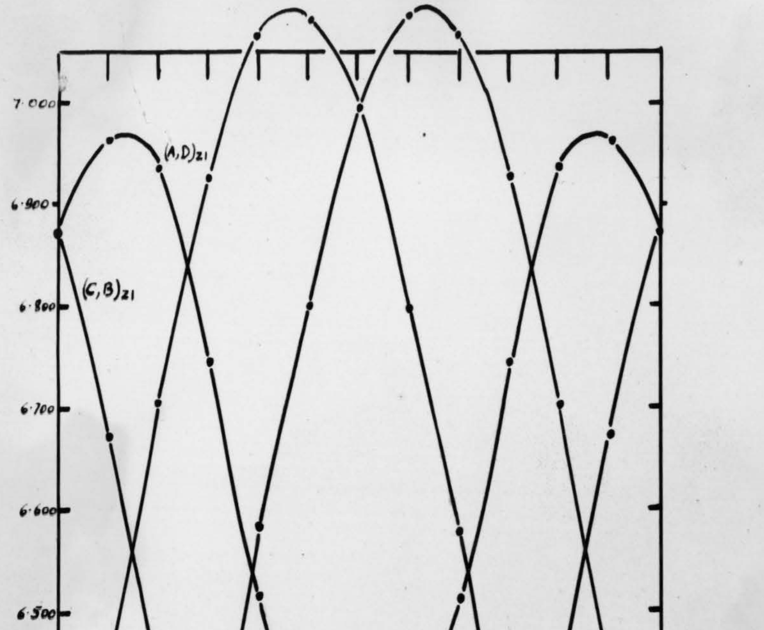

Fig 15. Frequency dependence of the position of satellites $\nu'$ and $\nu''$ on angular orientation of the crystal, Z-rotation.

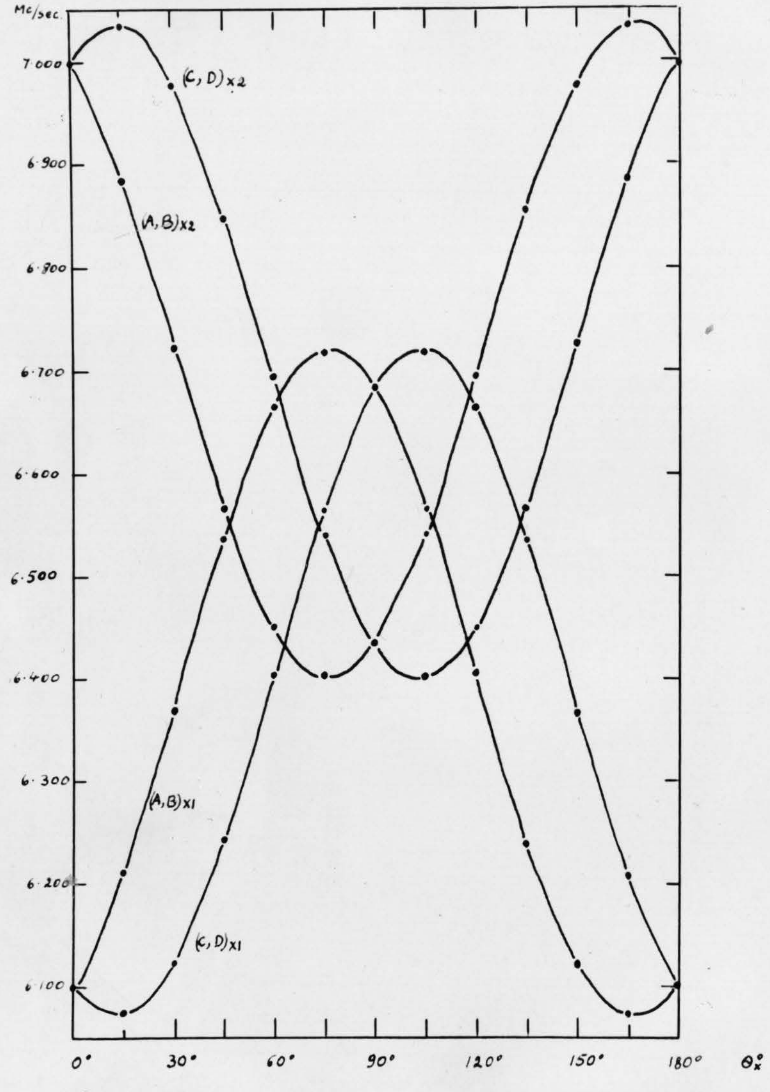

Fig. 16. Frequency dependence of the position of satellites $\nu'$ and $\nu''$ on angular orientation of the crystal, X-rotation.

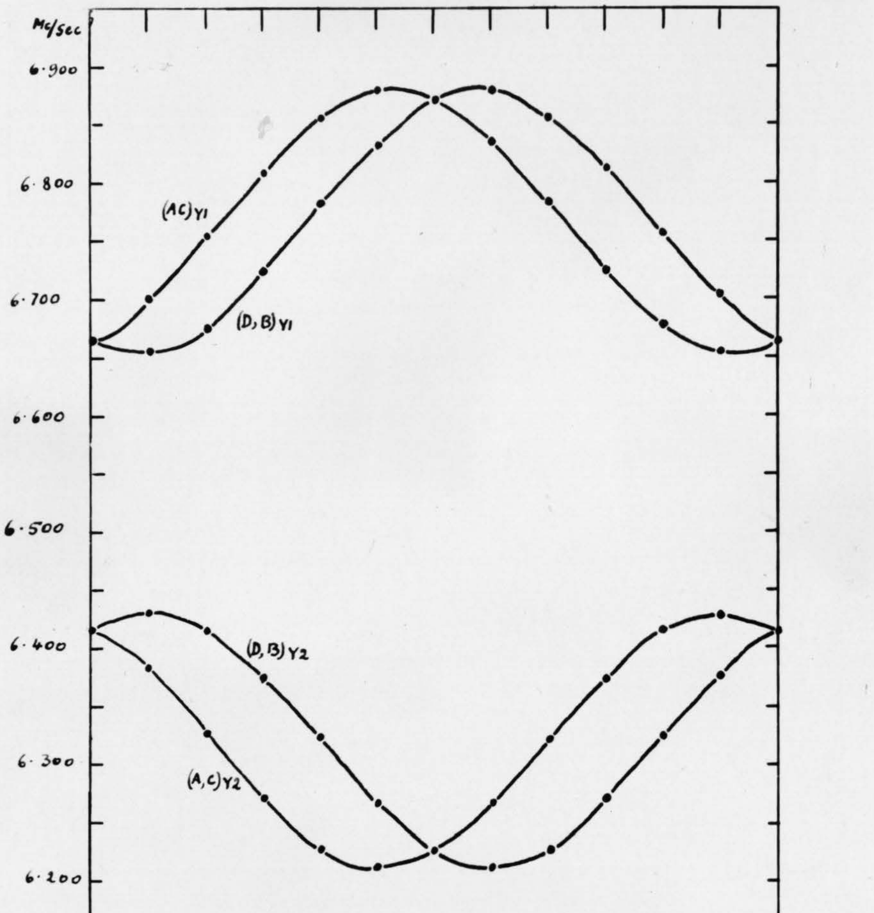

Fig 17. Frequency dependence of the position of satellites $\nu'$ and $\nu''$ on angular orientation of the crystal, Y-rotation.

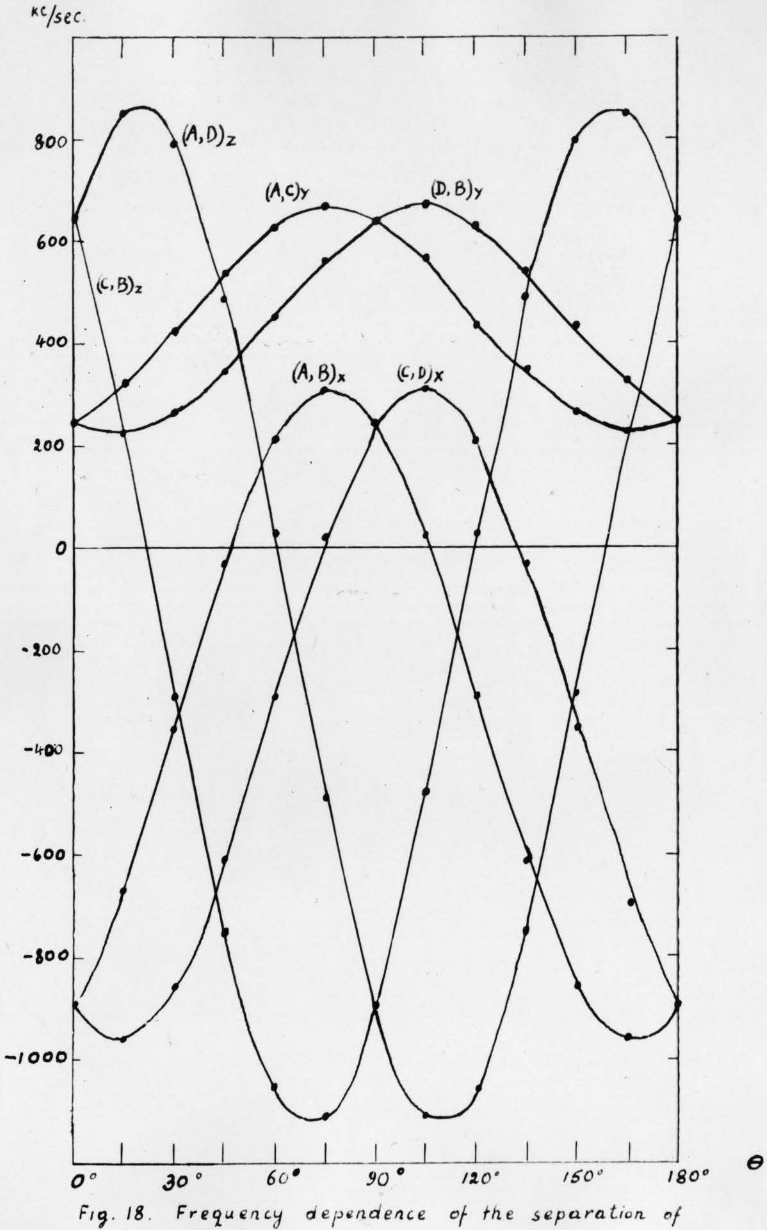

Fig. 18. Frequency dependence of the separation of satellites, ($\nu' - \nu''$), on angular position of the crystal.

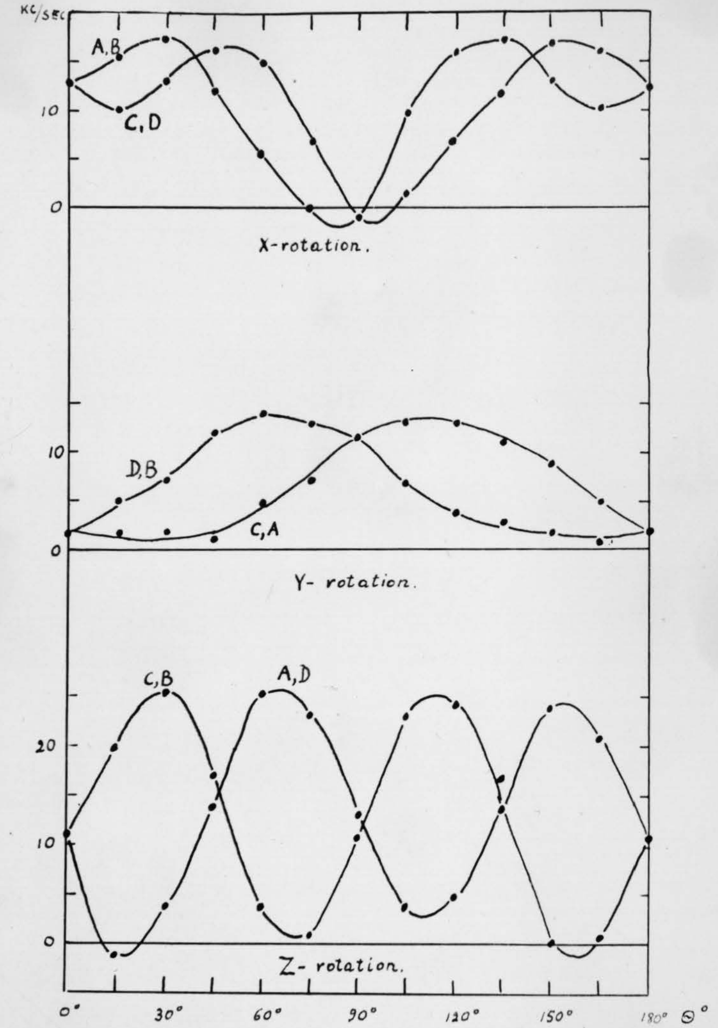

Fig. 19. Dependence of the shift of the "centre of gravity" of of satellites from the unperturbed frequency, $(\nu'+\nu'')/2 - \nu_0$, on angular position of the crystal.

## TABLE II

### Separation of Satellites, $\nu' - \nu''$, in Kc./Sec.

| | Site | 0° | 15° | 30° | 45° | 60° | 75° | 90° | 105° | 120° | 135° | 150° | 165° |
|---|---|---|---|---|---|---|---|---|---|---|---|---|---|
| X | C, D | -893 | -960 | -856 | -615 | -289 | +22 | 247 | 316 | 212 | -27 | -351 | -669 |
| | A, B | -893 | -676 | -358 | -29 | +213 | +317 | +247 | +26 | -292 | -605 | -855 | -959 |
| Y | D, B | 248 | 226 | 262 | 345 | 458 | 565 | 643 | 667 | 629 | 543 | 435 | 327 |
| | A, C | 248 | 321 | 429 | 540 | 627 | 668 | 643 | 567 | 463 | 349 | 264 | 227 |
| Z | C, B | 642 | 228 | -286 | -751 | -1050 | -1102 | -892 | -479 | 31 | 496 | 799 | 849 |
| | A, D | 642 | 855 | 798 | 492 | +30 | -483 | -892 | -1105 | -1049 | -746 | -282 | +230 |

# TABLE III

## The Shift of the Centre of Gravity of the Satellites $\frac{\nu' + \nu''}{2} - \nu_o$ and of the Central Component $\nu_c - \nu_o$ from the Unperturbed Frequency, $\nu_o$

| Rotation | | Site | 0° | 15° | 30° | 45° | 60° | 75° | 90° | 105° | 120° | 135° | 150° | 165° |
|---|---|---|---|---|---|---|---|---|---|---|---|---|---|---|
| X | $\frac{' + ''}{2} - {}_o$ | A, B | 13 | 15 | 17 | 12 | 6 | 1 | -1 | 10 | 16 | 17 | 13 | 10 |
| | | C, D | 13 | 10 | 13 | 16 | 15 | 0 | -1 | +2 | 7 | 12 | 17 | 16 |
| | $c - o$ | | 12 | 12 | 10 | -4 | +8 | 1 | -12 | -2 | -7 | -1 | -10 | -10 |
| | | | | | | -11 | -7 | -13 | | -14 | -7 | -10 | | |
| Y | $\frac{' + ''}{2} - {}_o$ | A, C | 2 | 2 | 2 | 1 | 5 | 7 | 12 | 13 | 13 | 11 | 9 | 5 |
| | | B, D | 2 | 5 | 7 | 12 | 14 | 13 | 12 | 7 | 4 | 3 | 2 | 1 |
| | $c - o$ | | -9 | -9 | -8 | 7 | -1 | -1 | -5 | -1 | -3 | -8 | -9 | -10 |
| | | | | -6 | 0 | -6 | -7 | -7 | | -9 | -8 | -5 | 0 | -6 |
| Z | $\frac{' + ''}{2} - {}_o$ | A, D | +11 | -1 | +4 | 14 | 27 | 23 | 11 | 4 | 5 | 17 | 24 | 21 |
| | | B, C | 11 | 20 | 16 | 14 | 4 | 1 | 11 | 23 | 24 | 14 | 0 | 1 |
| | $c - o$ | | -3 | +6 | +3 | -14 | -6 | -3 | -13 | -1 | -6 | -13 | +1 | +5 |
| | | | -24 | -24 | -25 | -17 | -21 | -24 | -14 | -24 | -26 | -16 | -27 | -20 |

in Figs. (15), (16) and (17). The significance of the rather complicated labelling scheme will become apparent near the end of the chapter. Each point on these curves represents an experimental observation but the solid lines joining the points were drawn only to help the reader to sort out the points.

The frequency differences with a common sign between the satellites $\nu'$ and $\nu''$ for the three rotations are tabulated in Table II. The common sign was chosen arbitrarily to make the separation of the satellites positive for the Z rotation at $\theta_z = 0$. This is an allowed procedure because a second rank tensor is not able to distinguish between a positive or negative direction. One can keep the signs consistent for the three rotations because the separations will be identical for the Z and Y rotations at $\theta_z = 0$ and $\theta_y = 90$ and for the Z and X rotations at $\theta_z = 90^\circ$ and $\theta_x = 0^\circ$. The results of Table II have been plotted in Fig. 18 in which the points represent experimental values and the solid lines are curves of the form $a + b \cos 2\theta + c \sin 2\theta$ which were fitted to the experimental points by the method of Whittaker and Robinson (8).

Second order effects were apparent, so the shift of the "centre of gravity" of the satellites and that of the central line have been tabulated in Table III and plotted in Fig. 19. In Fig. 19 the points represent experimental values but the solid lines have been drawn merely to aid the eye in joining up the points.

For a detailed numerical analysis the curves were fitted to the experimental points of Tables II and III by the 12 point analysis of Whittaker and Robinson (8) which amounts to fitting the experimental points to a curve of the form:

$$Y = \sum_{n=0}^{5} C_n \cos n\theta + \sum_{n=1}^{6} \sin n\theta$$

Before proceeding further one point needs to be explained. The theory of Chapter I of this section predicts that the measurements on the spectrum done at $\theta$ and at $\theta + 180$ should be identical. This amounts to saying that every curve shown in this chapter should be periodic with a period of 180°; consequently, measurements at $\theta$ and at $(180 + \theta)$ have been averaged and inserted under $\theta$.

The Fourrier analysis of the experimental points for the separation of the satellites showed that all the coefficients of higher order than the second are negligible (less than 0.5 kc./sec.) or that the general curve of Equation 34 reduces to the form:

$$a + b \cos 2\theta + c \sin 2\theta$$

as required by Equation 17. Also for the shift of the "centre of gravity" of the satellites, all coefficients of higher order than the fourth are negligible so that the curve reduces to a form:

$$p + n \cos 2\theta + r \sin 2\theta + u \cos 4\theta + v \sin 4\theta$$

as required by Equation 18. .

Once the Fourrier coefficients of the experimental curves have been obtained, the set of tensor components $\frac{C_z}{\phi_{zz}} \phi_{ij} = \psi_{ij}$ in the X, Y, Z co-ordinate system can ordinarily be calculated in a straight forward way using Equations (19), (20) and (21). However, in this case, the existence of the three mutually perpendicular two-fold rotation axes complicates matter because it is not immediately obvious which set of curves to associate with a single $Na^{23}$ site. First we make use of our knowledge that the eigenvalues for each of the four sites must be identical. This requires that a and b of Equation (17) must be identical for the four sites.

## TABLE lVa

## First Order Experimental Fourrier Coefficients

## in Kc./Sec.

| Site | Rotation | a | b | c |
|---|---|---|---|---|
| C, D | X | -321.9 | -568.3 | -291.9 |
| D, B | Y | 445.7 | -196.6 | - 99.7 |
| C, B | Z | -126.3 | 767.5 | -624.3 |
| A, B | X | -322.0 | -572.0 | 287.0 |
| A, C | Y | 445.6 | -197.3 | 95.6 |
| A, D | Z | -125.8 | 769.9 | 622.1 |

## TABLE IVb

## Experimental Second Order Fourrier Coefficients for the Sites A, B, C, D in Kc./Sec.

| Site | n | p | r | u | v | Rotation |
|---|---|---|---|---|---|---|
| A, B | 10.6 | 5.1 | -2.1 | -4.2 | 4.1 | X |
| A, C | 6.8 | -6.1 | -1.9 | 0.5 | 0.2 | Y |
| A, D | 12.5 | -1.4 | -1 | 2.6 | -12.1 | Z |
| C, D | 10 | 6.5 | +0.5 | -4.8 | -2.4 | X |
| D, B | 5.2 | -4.5 | +4.6 | -0.1 | -1.2 | Y |
| C, B | 12.7 | -0.6 | +1.1 | -2.25 | 12.6 | Z |

## TABLE V

### The Components of the Tensor $\Psi_{ij} = \frac{C_z}{\phi_{zz}} \phi_{ij}$

| Site | Rotation | XX | YY | ZZ | ZY | XZ | YX |
|---|---|---|---|---|---|---|---|
| | X | 644.0 | -894.0 | 250.0 | -287.9 | --- | --- |
| A | Y | 641.9 | -891.2 | 248.3 | --- | -95.6 | --- |
| | Z | 644.1 | -895.7 | 251.6 | --- | --- | -622.1 |
| Average | | 643.3 | -893.6 | 250.0 | -287.9 | -95.6 | -622.1 |
| | X | 644.0 | -894.0 | 250.0 | -287.9 | --- | --- |
| B | Y | 642.3 | -891.4 | 249.1 | --- | 99.7 | --- |
| | Z | 641.2 | -893.8 | 252.6 | --- | --- | 624.3 |
| Average | | 642.5 | -893.1 | 250.6 | -287.9 | 99.7 | 624.3 |
| | X | 643.8 | -890.2 | 246.4 | 291.9 | --- | --- |
| C | Y | 641.9 | -891.2 | 248.3 | --- | -95.6 | --- |
| | Z | 641.2 | -893.8 | 252.6 | --- | --- | 624.3 |
| Average | | 642.3 | -891.7 | 249.1 | 291.9 | -95.6 | 624.3 |
| | X | 643.8 | -890.2 | 246.4 | 291.9 | --- | --- |
| D | Y | 642.3 | -891.4 | 249.1 | --- | 99.7 | --- |
| | Z | 644.1 | -895.7 | 251.6 | --- | --- | -622.1 |
| Average | | 643.4 | -892.4 | 249.0 | 291.9 | 99.7 | -622.1 |

## TABLE VI

## The Principal Values of the Tensor $\psi_{ij}$, the Coupling Constants $C_z$ and the Asymmetry Parameters, $\eta$

| Site | $\gamma_1$ | $\gamma_2$ | $\gamma_3$ | $C_z$ | $\eta$ |
|---|---|---|---|---|---|
| A | -314.4 | -863.9 | +1178.1 | 1178.1 | 0.4664 |
| B | -315.5 | -864.3 | +1179.8 | 1179.8 | 0.4651 |
| C | -314.9 | -864.6 | +1179.5 | 1179.5 | 0.4660 |
| D | -311.6 | -866.6 | +1178.4 | 1178.4 | 0.4671 |
| Average | --- | --- | --- | 1179.0 | 0.4661 |

The problem then is to associate the three curves from Table IVa with each of the four sites called, say, A, B, C, D in such a way that a and b will be the same for the four $Na^{23}$ sites. Since only the C coefficients differ, and then only in sign, for the two curves obtained for each of the three rotations, the problem reduces to obtaining the combinations of curves which predict the same sign for all the sites for the triple product $\psi_{xy}$, $\psi_{xz}$, $\psi_{zx}$ which enters into b of Equation 27b. It turns out that, using the above information, there are two possible combinations. They are:

| | | | |
|---|---|---|---|
| A | B | A | B |
| C | D | C | D |
| $C_x, C_y, C_z$ is negative | | $C_x, C_y, C_z$ is positive | |

The first combination leads always to a positive sign for the triple product* $\psi_{xy}$, $\psi_{yz}$, $\psi_{zx}$ and the second combination to a negative sign. Only one combination can be the correct one. A study of the second order effects which cause the shift of the "centre of gravity" of the satellites removes this uncertainty. A study of the Fourrier coefficients r and v in Table IVb leads to the conclusion that the second of the above combinations, i.e., the one which leads to the negative sign in front of the product, is the correct one. The relations (19), (20) and (21) were then used to obtain the components of the tensor $\psi_{ij}$ in the X, Y, Z co-ordinate system for each of the four sites and these have been listed in Table V. These tensors were then diagonalised in the ordinary way to yield the eigenvalues which are listed in Table VI. The direction cosines of the

---

*Note that the relation: $C_i = -\psi_{jk}$ holds.

## TABLE VII

## The Direction Cosines of the Principal Axes (x, y, z) of the Tensor $\psi_{ij}$ with Respect to the Axes (X, Y, Z)

| Site | | x | y | z |
|---|---|---|---|---|
| | X | 0.0793 | 0.0380 | 0.3259 |
| A | Y | 0.1923 | -0.3415 | 0.9224 |
| | Z | -0.9781 | 0.0589 | 0.2072 |
| | X | -0.0738 | -0.9415 | -0.3269 |
| B | Y | 0.1948 | -0.3358 | 0.9210 |
| | Z | -0.9780 | 0.0083 | 0.2117 |
| | X | +0.0834 | 0.9390 | 0.3268 |
| C | Y | -0.1936 | 0.3424 | -0.9216 |
| | Z | -0.9787 | 0.0442 | 0.2097 |
| | X | -0.0762 | -0.8262 | -0.3265 |
| D | Y | -0.1968 | 0.4157 | -0.9229 |
| | Z | -0.9775 | 0.3797 | 0.2040 |

principal axes (x, y, z) with respect to the (X, Y, Z) frame of reference are listed in Table VII. They were calculated using the relationships (32) and (33) of Chapter I of this section.

## CHAPTER IV

This work gives the only available information about the $Na^{23}$ sites in $NaH_2PO_4.2H_2O$ crystals, namely, the quadrupole coupling constant, $\frac{e^2qQ}{h}$ = 1179 ± 3 kc./sec., the asymmetry parameters $\eta = 0.466 \pm 0.010$ and the direction cosines of the principal axes of the electric field gradient tensor listed in Table VII, Chapter III of this section.

The structure of $NaH_2PO_4.2H_2O$ has not been elucidated by X-ray technique or any other method, consequently the above results cannot be interpreted quantitatively in terms of chemical bonds. However, if one makes the use of the numerical value for the nuclear quadrupole moment (10) as being equal to 0.100 ± .003 barns, one can obtain an explicit value of $\phi_{z'z'} = eq$ from the quadrupole coupling constant evaluated from experimental observations. The value of $\phi_{z'z'}$ is thus found to be $1.63 \times 10^{14}$ esu/cm$^2$ . This numerical value of $\phi_{z'z'}$ is of the order of magnitude that one would expect for ionic bonds if one allows a factor which would decrease this value due to polarization introduced by Dailey and Townes (11). This can be compared to the value of $2.6 \times 10^{14}$ esu/cm$^2$ for $\phi_{z'z'}$ at $Al^{27}$ sites in spodumene found by Petch et al. The polarization induced by $Al^{27}$ electrons has again not been accounted for.

Recently, Bersohn (13) calculated the quadrupole polarization factor for $Na^{23}$ sites in the cubic $NaNO_3$ and $NaClO_3$. The theoretical expression is: $\frac{eqQ}{h} = \frac{e^2}{h a^3}(1-\gamma_\infty)Q(C_1+C_2 z)$ where a is unit cell length, ze is the charge at Cl or N atom respectively, $C_1$ and $C_2$ are constants for each $NaNO_3$ and $NaClO_3$ crystals. They find that instead of using Q for quadrupole moment of $Na^{23}$, one should use $(1 - \gamma\ )Q$ to account for the polarization of $Na^{+}$ ions. Thus, they find that $(1 - \gamma\ )Q = 0.556$ barns as compared to 0.10 barns as the value of Q for $Na^{23}$ nuclei. Thus, the value of $\phi_{z'z'}$ for $Na^{23}$ nuclei surrounded by a cubic crystal lattice is reduced by a factor of 5.56 due to polarization. One would expect that if one takes the account of polarization the numerical value of $\phi_{z'z'}$ found in this work would be reduced by a factor of the order of 5.

This work confirms moreover the existence of the 3 mutually perpendicular two-fold rotation axes coinciding with the crystallographic axes of $NaH_2PO_4.2H_2O$ crystals. This information is therefore consistent with the $P_{222}$ symmetry drawn from morphological data. This experiment shows, in particular, that there are four unequivalent $Na^{23}$ sites which have identical asymmetry parameters and identical quadrupole coupling constants but different values for the direction cosines of the principal axes of the electric field gradient tensor as listed in Table VII of previous chapter. The twelve-line spectrum observed results from superposition of the four three-line spectra belonging to the four uneuivalent $Na^{23}$ sites in the unit cell of $NaH_2PO_4.2H_2O$.

The results of this experiment indicate once again how useful are the second order effects in sorting out the spectrum. In fact, the second order effect was essential in sorting out the spectrum in this particular case dealing with a crystal having three mutually perpendicular two-fold rotation axes. The information gained from the second order effect was far too inaccurate for quantitative computations. The first order effects for the X, Y, and Z rotations, however, give sufficient data to carry out quantitative analysis of the spectra.

By virtue of its high symmetry the value of the quadrupole coupling constant of $Na^{23}$ sites in $NaH_2PO_4.2H_2O$ can be determined accurately. These crystals are therefore admirably suited for studying the effect of temperature on quadrupole coupling constant. This we plan to investigate in the near future.

## REFERENCES TO SECTION I

(1) P. Curie, Bull. Soc. Franc. Mineral., 8, 145, 1885.

(2) R. Marc and A. Ritzel, Z. Physik. Chem., 76, 584, 1911.

(3) A. Valeton, Z. Krist., 59, 135, 335, 1934.

(4) A. A. Noyes and W. R. Whitney, Z. Physik. Chem., 23, 689, 1897

(5) W. Nerust, Z. Physik. Chem., 47, 52, 1909.

(6) A. Berthoud, J. Chim. Phys., 10, 624, 1904.

(7) P. Niggli, Z. Anorg. Chem., 110, 55, 1920.

(8) W. Kossel, Jahresber. Math.-Physik. Klasse, 135, 1927.

(9) I. N. Stranski, Z. Physik. Chem., 136, 259, 1928.

(10) M. Born, "Atomtheorie des festes Zustances" from Encyklopaedie der Mathematischen Wissenshaft Leipzig, Teubner, 1923, p. 746.

(11) S. Ashton and J. Wilson, Am. J. Sci., 13, 209, 1927.

## REFERENCES TO SECTION II

(1) G. M. Volkoff, H. E. Petch, D. W. Smelie, Can. J. Phys., 30, 270, 1952.

(2) H. E. Petch, N. G. Cranna, G. M. Volkoff, Can. J. Phys., 31, 837, 1953.

(3) H. H. Waterman, G. M. Volkoff, Can. J. Phys., 33, 156, 1955.

(4) R. V. Pound, Phys. Rev., 79, 685, 1950.

(5) R. Bersohn, J. Chem. Phys., 20, 1505, 1952.

(6) G. M. Volkoff, Can. J. Phys., 31, 820, 1953.

(7) E. U. Condon and G. H. Shortley, "The Theory of Atomic Spectra", Cambridge University Press, 1953, Chapter III.

(8) E. Whittaker and G. Robinson, "The Calculus of Observations", Blackie and Son Ltd., London, 1948.

(9) K. A. Lines, "A Nuclear Magnetic Resonance Spectrometer", M.Sc. Thesis, Department of Physics, McMaster University.

(10) H. Lew, Phys. Rev., 76, 1086, 1949.

(11) C. H. Townes and B. P. Dailey, J. Chem. Phys., 20, 35, 1952.

(12) H. E. Petch, N. G. Cranna and G. M. Volkoff, Can. J. Phys., 31, 837, 1953.

(13) R. Bersohn, Washington meeting of the A. P. S., 1956.